ORNL/TM-2018/876

Dynamic Systems Models for Informing Licensing & Safeguards Investigations of Molten Salt Reactors

M. S. Greenwood
B. Betzler
L. Qualls

June 2018

**Approved for public release.
Distribution is unlimited.**

OAK RIDGE NATIONAL LABORATORY
MANAGED BY UT-BATTELLE FOR THE US DEPARTMENT OF ENERGY

ORNL/TM-2018/876

Reactor & Nuclear Systems Division

Dynamic Systems Models for Informing Licensing & Safeguards Investigations of Molten Salt Reactors

M. S. Greenwood, B. Betzler, L. Qualls

Date Published: June 2018

Prepared by
OAK RIDGE NATIONAL LABORATORY
Oak Ridge, TN 37831-6283
managed by
UT-BATTELLE, LLC
for the
US DEPARTMENT OF ENERGY
under contract DE-AC05-00OR22725

CONTENTS

CONTENTS iii
LIST OF TABLES v
LIST OF FIGURES vii
ABSTRACT 1
1. INTRODUCTION 1
    1.1 Terminology 2
2. CRITERIA FOR DYNAMIC MODELS 3
    2.1 Licensing 3
    2.2 Safeguards 4
    2.3 Additional Considerations 5
    2.4 Summary of Dynamic Model Criteria 5
3. CONCEPT DESCRIPTION 7
    3.1 Primary Fuel Loop 7
        3.1.1 Reactor 8
        3.1.2 Fuel Pumps 13
        3.1.3 Primary Heat Exchangers 14
    3.2 Primary Coolant Loop 14
    3.3 Power Cycle 15
    3.4 Residual Heat Removal System 15
    3.5 Off-Gas System 17
    3.6 Concept Description Summary 17
4. DYNAMIC MODEL 18
    4.1 Primary Fuel Loop 23
        4.1.1 Trace Substances 25
    4.2 Primary Coolant Loop 25
    4.3 Power Cycle Balance of Plant 25
    4.4 Off-Gas System, Drain Tank, and Decay Heat Removal System 25
        4.4.1 Off-Gas System 25
        4.4.2 Drain Tank 26
        4.4.3 Decay Heat Removal 26
    4.5 Media Thermophysical Properties 26
        4.5.1 Fuel Salt 26
        4.5.2 Coolant Salt 27
        4.5.3 Decay Heat Removal System Salt 27
        4.5.4 Power System Balance of Plant 28
        4.5.5 Graphite 28
        4.5.6 Alloy-N 28
        4.5.7 Carbon Adsorber Bed 28
    4.6 Pressure Loss and Heat & Mass Transfer Correlations 29
        4.6.1 Pressure Loss 29
        4.6.2 Heat Correlations 29
        4.6.3 Mass Transfer Correlations 29
    4.7 Reactor Kinetics, Fission Product, and Tritium Properties 30
        4.7.1 Power Profile 31
        4.7.2 Temperature Reactivity Feedback 31
        4.7.3 Neutron Precursor Groups 32

4.7.4 Fission Source 32
4.7.5 Fission Product Groups 32
4.7.6 Tritium 33
5. RESULTS 35
5.1 Case 1 – Steady-State Behavior 35
5.2 Case 2 – Behavior Under PFL Pump Trip Scenarios 38
5.3 Case 3 – Simulation in Change of Fissile Material 46
6. CONTINUING AND FUTURE WORK 49
6.1 Application to Other MSR Types 50
6.2 Parametric and Sensitivity Studies 51
7. SUMMARY 53
8. REFERENCES 55

LIST OF TABLES

Table 1. Primary heat exchangers nominal operating conditions (Table 2 from Bettis, Alexander, and Watts 1972) 14
Table 2. Secondary heat exchangers nominal operating conditions 15
Table 3. NaK-water tank heat exchanger nominal operating conditions 16
Table 4. Summary of mass and volumes of graphite and salt in the primary fuel and coolant loops 19
Table 5. Summary of reactor components 20
Table 6. Summary of primary fuel loop components (excluding reactor) 21
Table 7. Summary of primary coolant loop components (excluding primary heat exchanger) 22
Table 8. Summary of off-gas and decay heat removal system components 23
Table 9. Specified thermophysical properties of a linear compressible implementation of fueled FLiBe (Temperature in K) 27
Table 10. Specified thermophysical properties of a linear compressible implementation of FLiBe (Temperature in K) 27
Table 11. Specified thermophysical properties of a linear compressible implementation of FLiBe (Temperature in K) 28
Table 12. Specified thermophysical properties of primary fuel loop graphite (Temperature in K) 28
Table 13. Specified thermophysical properties of Alloy-N (Temperature in K) 28
Table 14. Specified thermophysical properties of charcoal adsorber bed 28
Table 15. Frictional pressure loss correlations for pipes 29
Table 16. Heat transfer correlations for pipes 29
Table 17. Arrhenius parameters for tritium diffusion 29
Table 18. Mass transfer to surfaces correlations for tritium. 30
Table 19. Solubility parameters for tritium diffusion at salt/solid interfaces 30
Table 20. Core temperature feedback parameters 31
Table 21. Summary of neutron precursor group parameters 32
Table 22. Summary of fission source parameters 32
Table 23. Fission product elemental groups 33
Table 24. Fission product half-life groups 33
Table 25. Summary of tritium parameters 34
Table 26. Case descriptions 35
Table 27. Steady-state simulation summary 35
Table 28. Steady-state inlet and outlet temperature of principle components (°C) 35
Table 29. Steady-state average core and reflector temperatures (°C) 35
Table 30. Steady-state pressures in PFL 36
Table 31. Steady-state flow rates 36
Table 32. Steady-state power in the core (decay heat does not include loop contribution) 36
Table 33. Steady-state heat rejection from decay heat removal system 36
Table 34. Tritium generation and release rate 36
Table 35. Case 2 – Scenario description 38
Table 36. Case 3 – Scenario description 46

LIST OF FIGURES

Figure 1. Terminology of high-level systems for salt-fueled MSRs. 2
Figure 2. High-level categorization of MSRs. 3
Figure 3. Simplified flowsheet of MSDR, a fluoride–salt-fueled thermal reactor. Not all flow loops are shown. 7
Figure 4. Depiction of reactor vessel geometry (Fig 2. from Bettis, Alexander, and Watts 1972, ORNL DWG 72-2829). 8
Figure 5. Reactor vessel geometry with dimensions (Fig 2. from Bettis, Alexander, and Watts 1972, ORNL DWG 72-2829). Dimensions are in inches and are approximate based on available information. 9
Figure 6. Approximate dimensions of inner and outer graphite reflector. Depiction is one of eight radial reflector sections, and the outer ring is the reactor vessel exterior wall. Dimensions are in inches. 10
Figure 7. Top view of axial reflector showing concentric rings of graphite with narrow fluid channels between rings and between smaller graphite blocks within rings (Fig. 4 from Bettis, Alexander, and Watts 1972, ORNL DWG 72-4030) 11
Figure 8. Reproduction of core cell (Fig. 7 from Bettis, Alexander, and Watts 1972, ORNL DWG 72-2830). Dimensions are in inches. The dashed magenta line indicates a unit cell. 11
Figure 9. Reproduction of control rod cell (Fig. 12 A-A from Bettis, Alexander, and Watts 1972, ORNL DWG 72-3576) with the exterior graphite matrix added. Dimensions are in inches. The dashed magenta line indicates a unit cell. 12
Figure 10. Reactor core and reflector plan (Fig. 6 from Bettis, Alexander, and Watts 1972, ORNL DWG 72-2826). 12
Figure 11. An example of a large sump-type fuel pump (Fig. 3.34 from Robertson 1971, ORNL DWG 96-6802). 13
Figure 12. Drain tank (Fig. 21 from Bettis, Alexander, and Watts 1972) 16
Figure 13. Dynamic model of the fluoride–salt-fueled, thermal reactor based 18
Figure 14. Dynamic model of the drain tank natural circulation decay heat removal system. 19
Figure 15. Characteristic geometry of the graphite blocks of the axial reflectors 24
Figure 16. Comparison of analytic (dashed line) and numeric (solid line) models of the generation and movement of neutron precursors in a salt-fueled MSR (Greenwood and Betzler In Review). 31
Figure 17. Steady-state temperature distribution as a function of position in the PFL. 37
Figure 18. Steady-state normalized concentrations distribution of select precursors as a function of position in the PFL. 38
Figure 19. Case 2 – Mass flow rate and loop transit time as a function of time. 39
Figure 20. Case 2 – Fission and decay heat as a function of time. 39
Figure 21. Case 2 – Average temperature of fuel salt and graphite as a function of time for the core (left) and radial reflector (right). 40
Figure 22. Case 2 – Maximum, average, and minimum fuel and graphite temperature in the core for each case scenario. 40
Figure 23. Case 2 – Core inlet pressure as a function of time. 41
Figure 24. Case 2 – PHX inlet and outlet temperature as a function of time (Tube = PFL; Shell = PCL). 41
Figure 25. Case 2 – SHX inlet and outlet temperature as a function of time (Tube = BOP; Shell = PCL). 42
Figure 26. Case 2 – Normalized tritium generation and release rate as a function of time. 42
Figure 27. Case 2 – Temperature for each scenario as a function of time and position. 43

Figure 28. Case 2 – Tritium concentration for each scenario as a function of time and position. 44
Figure 29. Case 2 – Neutron precursor group 5 concentration for each scenario as a function of time and position. 45
Figure 30. Case 2 – ^{135}Xe concentration for each scenario as a function of time and position. 46
Figure 31. Case 3 – Fission and decay heat as a function of time. 47
Figure 32. Case 3 – Average temperature of fuel salt and graphite as a function of time for the core (left) and radial reflector (right). 47
Figure 33. Case 3 – Core inlet pressure as a function of time. 48
Figure 34. Example of one method to modify the fluid and heat transfer correlation used in components. 51
Figure 35. Example of a method to replace an existing component with a different component. 51

ABSTRACT

Fluid-fueled molten salt nuclear reactors (MSRs) have recently gained significant interest. As with all reactors, modeling and simulation are key factors for advanced reactor design and licensing and will be required for the deployment of MSRs. However, there are significant gaps between simulation capabilities and system behavior for MSRs. This paper presents a system model of an MSR based on the Molten Salt Demonstration Reactor. The model includes important physics specific to MSRs, such as fission product and tritium transport, as well as reactivity feedback.

1. INTRODUCTION

The past few years have seen a significant increase in the interest of advanced fluid-fueled molten salt reactor (MSR) systems. A *fluid-fueled reactor* is any reactor in which the fissile material is in liquid form. Reactors such as MSRs could represent a revolutionary shift in the way nuclear power is implemented, and as a broad class of reactors, they have the potential to directly fulfill many US energy policy objectives. Although concept development is the responsibility of vendors, US Department of Energy (DOE) laboratories have a role providing understanding and assistance in many critical areas. For MSRs, this includes salt production, salt chemistry, corrosion and control studies, materials qualifications, instrumentation, decay heat removal, operations and maintenance, and radionuclide inventory tracking, among others. These areas are all related to licensing for MSRs, which is the ultimate goal.

Modeling and simulation are key for advanced reactor design and licensing. However, MSRs do not yet have any tools approved for this purpose. The Molten Salt Reactor Experiment (MSRE) design and licensing process relied on several in-house custom codes such as MURGATROYD (Haubenreich and Engel 1962) to investigate safety cases and reactor performance. There are several modeling and simulation capabilities that can be used to investigate various aspects of nuclear reactors, including those provided by the Consortium for Advanced Simulation of Light Water Reactors (CASL) and the Nuclear Energy Advanced Modeling and Simulation Program (NEAMS). However, these capabilities have not been approved as licensing tools. Many capabilities from these and other programs are being adapted, or new ones are being created (Touran et al. 2017) to address the needs of advanced nuclear reactors and to ultimately generate tools that can be used for design and licensing of advanced reactors. Even so, significant technological gaps are preventing rapid development of these tools. These gaps include lack of data or difficulties in adapting legacy code intended for alternative applications such as light water reactor (LWR) technologies.

Development of a low-fidelity system-level model was identified as a straightforward way to identify needs and gaps in data and simulation capabilities and identify and investigation various phenomena that may impact safety and licensing. Identification of needs and gaps will inform required modifications to existing capabilities, help direct experimental data generation, and assist in requirement generation for modern high-fidelity code generation. This report details a generic system-level model of a thermal fluoride salt-fueled MSR that was created using the Modelica-based TRANSFORM tool (Greenwood 2017) developed at ORNL. The generic nature of the model's implementation also makes it appropriate for evaluating other designs, including salt-cooled designs and other salt-fueled designs (e.g., chloride). This report and the associated modeling:

1. Establish physics-based model(s) capable of capturing appropriate behaviors to advance the understanding of the physical behaviors of MSRs.
2. Contribute information to help identify technological needs and modeling and simulation gaps needed for development of MSRs, with focus on needs for licensing and safeguards.

This report outlines the rationale for the down-selection of the reactor concept for dynamic modeling and presents the elements required in the model for licensing and safeguards understanding of MSRs. Specific details (e.g., components, sizes, parameters, assumptions) of the modeled system are then presented. The model is described, and a few simulations of the model are presented to provide a preliminary idea of the type of information available and types of scenarios that can be studied using this system-level modeling tool. The report concludes with (1) a summary of identified technology gaps in MSR understanding, data, etc., that were gleaned from the creation of the dynamic models, and (2) details on proposed follow-on work.

1.1 TERMINOLOGY

For consistency and clarity to the state of the art, this document adopts the terminology used in American Nuclear Society (ANS) Standard 20.2, "Nuclear Safety Design Criteria and Functional Performance Requirements for Liquid-Fuel Molten-Salt Reactor Nuclear Power Plants." Figure 1 illustrates the terminology of the high-level systems for integral and loop type MSR designs. If additional coolant loops exist between the first and the ultimate heat sink (e.g., steam power cycle) they are designated as second, third, etc. coolant loops.

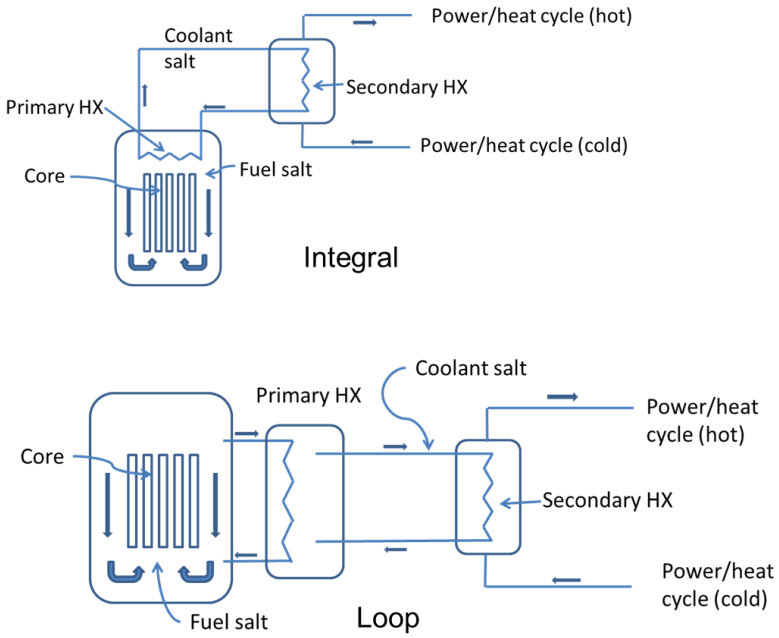

Figure 1. Terminology of high-level systems for salt-fueled MSRs.

2. CRITERIA FOR DYNAMIC MODELS

The number of possible salts and material combinations that can be used in MSRs leads to a broad range of potential MSR concepts. However, for a basic representation, MSRs can be classified into the following groups:

1. **Salt-cooled reactors**: A solid fuel undergoes fission and is cooled by a separate non-fueled primary system salt
2. **Salt-fueled reactors:** A flowing fueled salt contains fissile material that fissions when in the core and flows throughout the primary system, serving as fuel and coolant.

Both salt-cooled and salt-fueled concepts can be fast, epithermal, or thermal spectrum reactors, with the primary categories loosely defined as salt-cooled fluoride, salt-fueled fluoride, and salt-fueled chloride-fast (Figure 2). Salt-cooled concepts of current interest are mainly thermal spectrum concepts that use fluoride salts as the primary coolant. This class of reactor, known as fluoride salt–cooled high-temperature reactors (FHRs), has been the subject of the majority of recent MSR research, including concept design studies at ORNL (Ingersoll and Forsberg 2004; Ingersoll 2005; Ingersoll, Forsberg, and MacDonald 2007; A. L. Qualls et al. 2016; A. Louis Qualls et al. 2017; Brown et al. 2017). Licensing paths and safeguards for salt-cooled concepts are more analogous to traditionally licensed reactor designs. Therefore, a salt-cooled MSR concept is not included as part of this modeling effort. Rather, the lower technology readiness level (TRL) and limited-to-no operational experience salt-fueled concepts are analyzed. However, salt-fueled and salt-cooled MSR concepts have many common technology needs, and it is expected that many of the methods and information obtained from dynamic models of salt-fueled models will also advance the science on salt-cooled concepts.

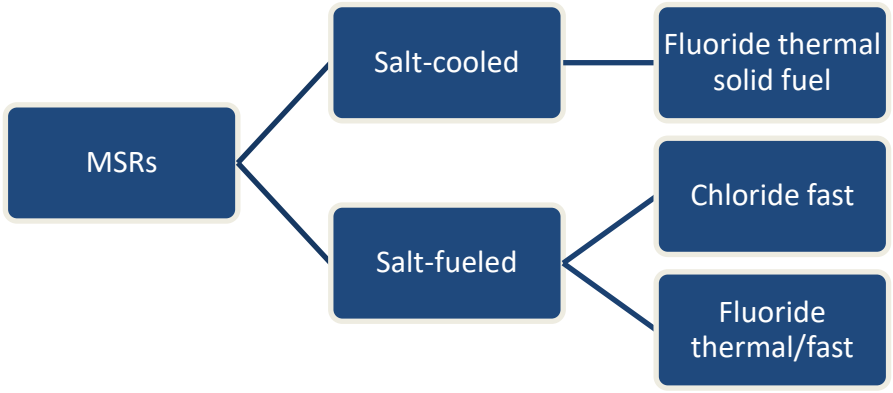

Figure 2. High-level categorization of MSRs.

Information critical for making modeling decisions (e.g., reasonable assumptions, necessary components, phenomenon to investigate) relies on the end use of the developed, dynamic models. Reactor commercialization has many critical areas that must be addressed. Two areas that must be addressed for commercialization of MSRs are: (1) licensing and (2) safeguards. Each area will be discussed to clarify needs from the dynamic model in accordance with the stated goals of this report.

2.1 LICENSING

US Nuclear Regulatory Commission (NRC) licensing processes are focused on fulfilling the mission to ensure the protection of public health and safety, common defense and security, and the environment (NRC 2010). Of primary importance are the types of radioactive sources and their pathways of exposure to site personal and the public. Current NRC regulation philosophy is predicated on nominally fixed fuel

forms (i.e., encapsulated solid fuel that can be readily accounted for). As such, there are several questions about how a salt-fueled system behaves, the multiple locations of source terms outside the core, and the method for quantifying the movement of the source terms, including qualification under transient accident scenarios. The questions are as follows:

1. What are the lifecycles of the radioactive materials in the systems?
2. What are the physical behaviors of source term elements?
3. Which source terms are important to safety analysis?
4. How can online refueling and/or salt processing mitigate excess reactivity concerns and/or potential accident consequences?

The modeling elements needed to begin answering these questions and to inform future experimental, modeling, and simulation work are as follows:

1. Allow source term tracking (some overlap with safeguards), including radioactive inventories and locations, source term generation and decay, release pathways, etc.
2. Include safety systems, including passive coolant systems, drain tanks, freeze valve, etc.
3. Include auxiliary systems that contain source terms such as off-gas, salt cleanup, drain tanks, core, salt sampling, etc.

2.2 SAFEGUARDS

The International Atomic Energy Agency (IAEA) safeguards objective is specified in Paragraph 28 of INFCIRC/153 (IAEA 1972) as:

> *the timely detection of diversion of significant quantities of nuclear material from peaceful nuclear activities to the manufacture of nuclear weapons or of other nuclear explosive devices or for purposes unknown, and deterrence of such diversion by the risk of early detection.*

An effective safeguards system for MSRs requires a deep scientific understanding of change detection—a clear understanding how the quantity, isotopic composition, and chemical/physical form of nuclear material changes with normal operational variations and anticipated operational occurrences. Furthermore, being able to clearly distinguish acceptable variations from changes due to nuclear material diversion scenarios is necessary to accurately detect undeclared activities via sensor integration at the system level.

A comprehensive safeguards approach has not been determined for MSRs. It is preferable to address safeguards needs during the design phase rather than retrofitting the plant to incorporate safeguards after it is commissioned. A safeguards by design approach will be most effective, as MSRs combine reactor and fuel cycle processes in a single facility. In particular, liquid-fueled MSRs challenge conventional safeguards measures, which currently draw strong distinctions between item and batch facilities. These distinctions are not as clear for MSRs. Some questions pertinent to addressing MSR safeguards are as follows:

1. What potential operations scenarios can change the amount of fissile material produced in an MSR, and what potential scenarios can change the quality and quantity of fissile material that is separated?
2. What signatures of off-normal changes vs. acceptable operational variations could indicate clandestine operations?
3. What are the interdependencies of the operational parameters and resulting signatures?

4. Where must instruments be placed to detect these changes?

Modeling requirements to enhance understanding of safeguards issues and to inform future experimental efforts and modeling and simulation work are as follows:

1. Include a salt process that diverts fuel-salt (e.g., off-gas system) or that otherwise modifies fuel composition (e.g., refueling) to allow for investigation of system behavior under different scenarios with safeguard implications
2. Enable stream condition identification (e.g., mass flow rate, source term, temperatures, pressures, etc.)

2.3 ADDITIONAL CONSIDERATIONS

Within the salt-fueled fluoride category, MSR historical operational experience lies with small salt-fueled, thermal spectrum demonstration reactors operated at ORNL (Rosenthal 2009). The Aircraft Reactor Experiment (ARE) used a fueled sodium-zirconium-uranium fluoride salt. The Molten Salt Reactor Experiment (MSRE) used a fluoride-based salt that included lithium, beryllium, and zirconium salts, in addition to fluorinated fissile materials in solution. MSRE operated with ^{235}U, ^{233}U, and ^{239}Pu as fissionable material, partially demonstrating the feasibility of both the uranium-plutonium and thorium-uranium fuel cycles. Available experimental data for comparison and the significant amount of documentation for fluoride salt-fueled thermal reactor systems (including data on balance of plant and auxiliary systems), combined with current commercial interest, make a realistic dynamic model of this system feasible. These data will likely have a significant impact on understanding the challenges that could occur in a real system.

Fast-spectrum salt-fueled concepts often use chloride salts and are perhaps the least mature of the MSR concepts. There is comparatively little historical experience with chloride-based reactor designs (Taube et al. 1978; Bulmer et al. 1956; Smith and Simmons 1974). The chloride salt–fueled fast reactor has an unrefined design space when compared to a thermal salt–fueled concept from the perspective of publicly available literature. However, chloride-salt systems offer the promise of a fast neutron spectrum for improved fissile resource utilization and actinide waste consumption. Following their initial core loads, breed-and-burn fast-spectrum MSRs can potentially avoid the requirement for uranium enrichment entirely. Furthermore, gaps in understanding of chloride-based systems, along with commercial interest, make a generic, system dynamic model of salt-fueled chloride fast reactor of special value in advancing the understanding of this system type. Therefore, the modeling for this work must be done in a manner that permits model creation of alternative MSR designs such as a fast salt-fueled chloride reactor.

2.4 SUMMARY OF DYNAMIC MODEL CRITERIA

The associated needs of licensing and safeguards, coupled with publicly available design information and commercial interests, form a design envelope which helps maximize the usefulness of the dynamic models presented in the report. Based on the discussion above, the criteria identified require that the following features be included in the dynamic models:

1. Precursor drift models that account for delayed neutron production throughout the primary loop and their reintroduction into the core
2. Radionuclide inventory accounting, including source term production, holdup, and release mechanism models
3. Thermal hydraulic analyses of sufficient fidelity to capture flow and power dynamics in salt-fueled concepts

4. Time-, temperature-, flux-, and flow-dependent materials, and salt interaction data, and models to predict corrosion, erosion, and irradiation effects
5. Modeled concepts that rely on existing data where possible to minimize development time while remaining relatively generic and applicable to modern MSR designs.

To achieve these modeling criteria, a fluoride salt-fueled thermal reactor concept was selected for development into a dynamic multiphysics model. Details of the concept, how it was modeled, and the model's behavior in scenarios illustrating the types of information available from the model are presented in the following sections.

3. CONCEPT DESCRIPTION

This section provides details on the guiding documents and theory behind the fluoride salt-fueled, thermal reactor concept which was selected and modeled. The Molten Salt Demonstration Reactor (MSDR) (Bettis, Alexander, and Watts 1972) provides the base design concept for the fluoride salt-fueled reactor dynamic model (Figure 3) with the exception that a U/Pu fuel salt is used rather than the Th fueled salt of the original concept. This concept has a nominal thermal output of 750 MWt. The purpose of the MSDR was to demonstrate the MSR concept on a semi-commercial scale while requiring little development of basic technology beyond that demonstrated in the MSRE. A significant advantage of basing the fluoride reactor concept on an existing ORNL design is attributable to detailed design document developed by researchers intimately familiar with the technology. The MSDR also leverages the work of the Molten Salt Breeder Reactor (MSBR) (Robertson 1971) for information on off-gas, chemistry, materials, neutron physics, fuel reprocessing, etc., which was also carefully documented. Furthermore, to reach the near-term deployment targets of modern vendors, this model was expected to provide information directly applicable to the development of commercial reactors by minimizing development needs and complication of systems—all elements that are expected from near-term vendors.

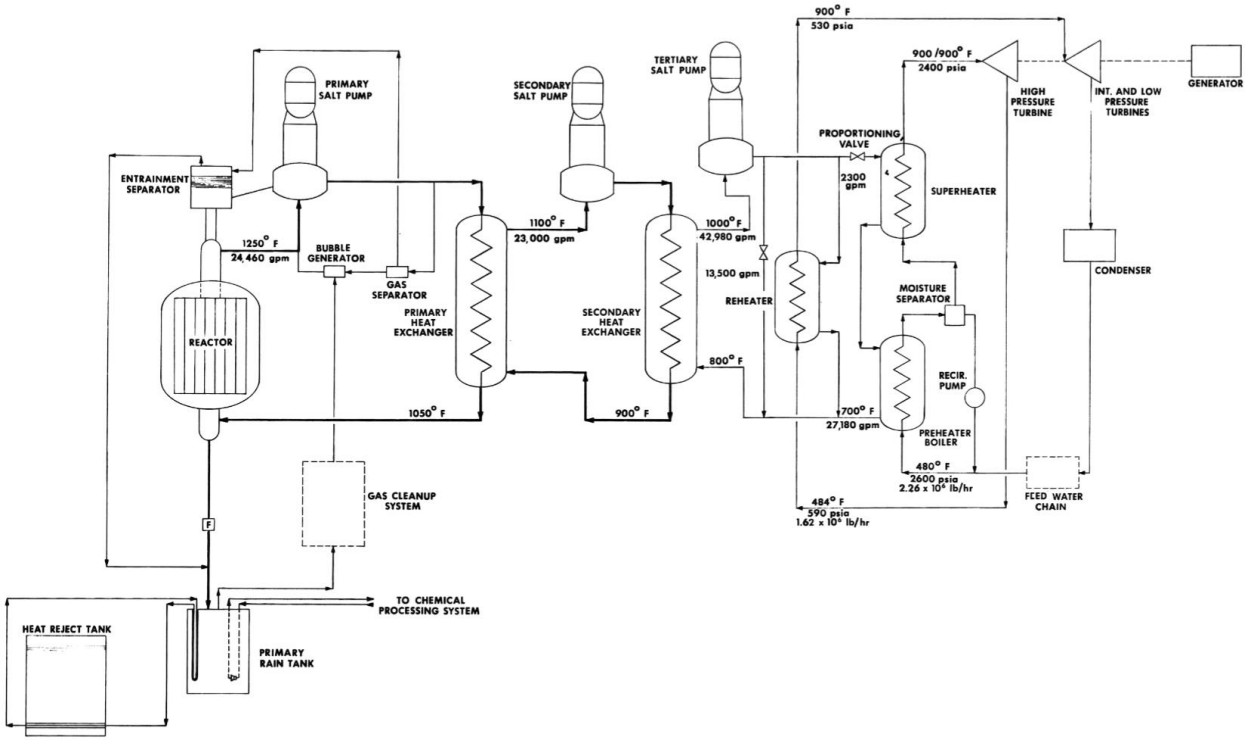

Figure 3. Simplified flowsheet of MSDR, a fluoride–salt-fueled thermal reactor. Not all flow loops are shown.

3.1 PRIMARY FUEL LOOP

The primary fuel loop is a 750 MWt forced flow loop-type system. The fuel salt is a U/Pu bearing molten FLiBe. The primary fuel loop consists of a single reactor core which branches to three heat exchanger loops from the top of the reactor and rejoins at a tee before the inlet of the reactor. Each heat exchanger loop has one pump and two heat exchangers. Auxiliary systems tightly coupled with the primary fuel loop are the residual heat removal system and the off-gas system. Due to these systems' importance and complexity, they are described in separate sections.

Careful consideration of the dimensions described by Bettis et al. (Bettis, Alexander, and Watts 1972) and the provided drawings indicate that some details are unclear, particularly regarding vessel and graphite size. Therefore, the dimensions provided here are best estimates made from available documentation.

3.1.1 Reactor

The reactor vessel is a cylindrical vessel with a height comparable to the diameter (26 × 32 ft.) with dished heads (Figure 4 and Figure 5).

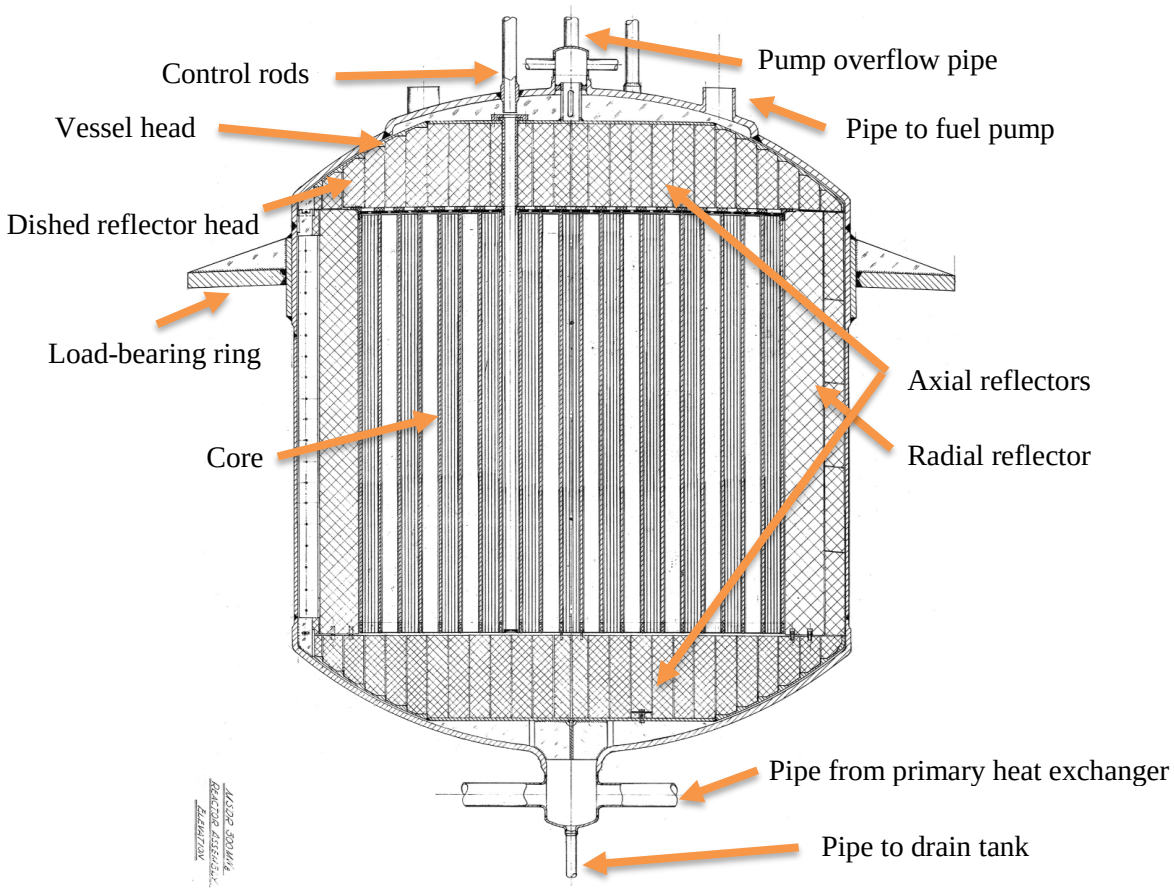

Figure 4. Depiction of reactor vessel geometry (Fig 2. from Bettis, Alexander, and Watts 1972, ORNL DWG 72-2829).

b

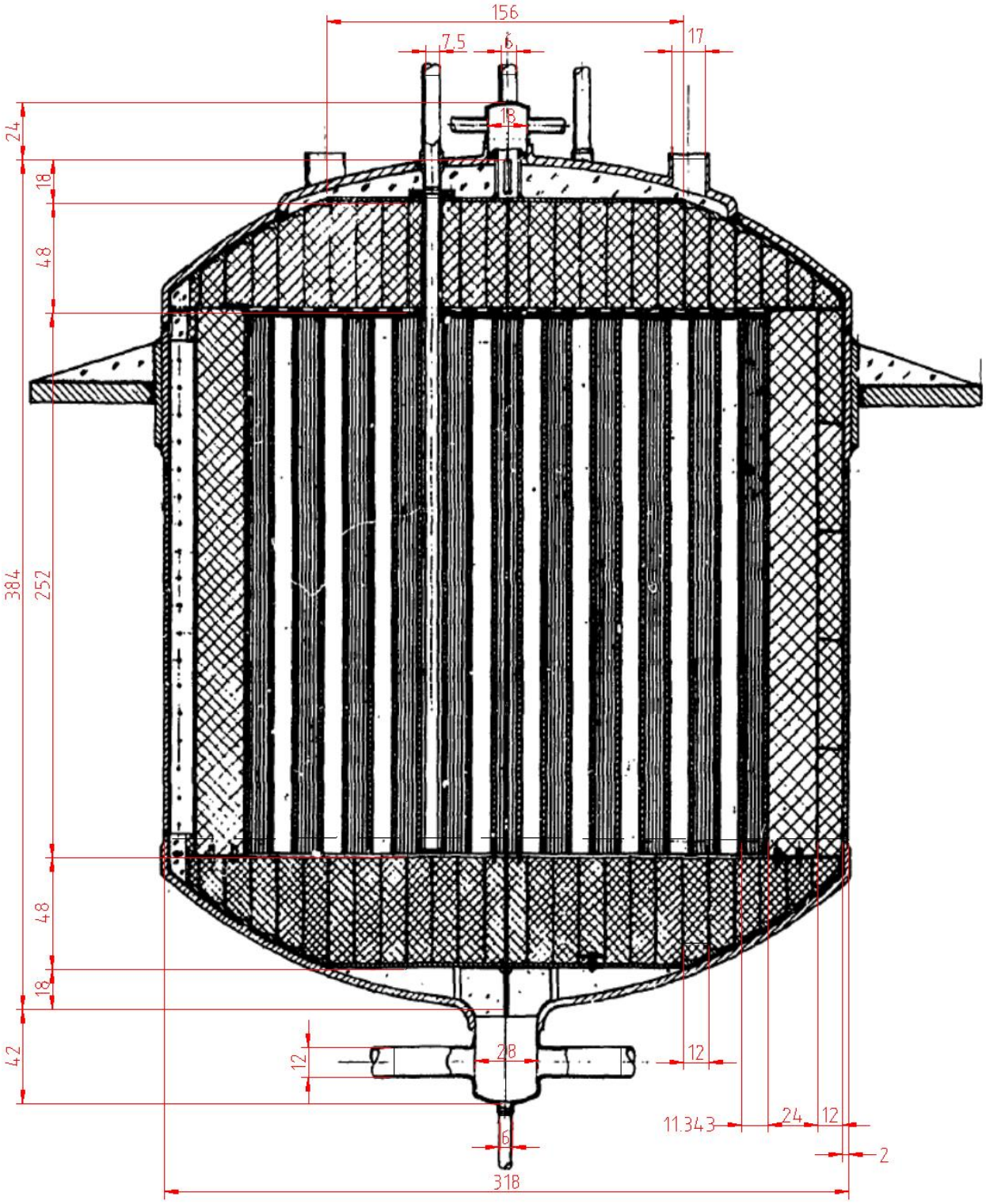

Figure 5. Reactor vessel geometry with dimensions (Fig 2. from Bettis, Alexander, and Watts 1972, ORNL DWG 72-2829). Dimensions are in inches and are approximate based on available information.

The interior of the reactor consists of a core region, axial and radial reflectors, and a small inlet and outlet plenum. The radial reflector consists of an inner and outer region of large graphite slabs spaced approximately 0.125 in. apart to allow a small flow of fuel salt to cool the graphite. The outer region consists of 10 × 3 × 1 ft. slabs stacked horizontally on one another and machined to be $^{1}/_{16}$ in. from the vessel wall. The inner region consists of 21 × 2 × 1 ft. graphite slabs stacked vertically adjacent to each other. Figure 6 provides a top view of the geometry of the radial reflector region.

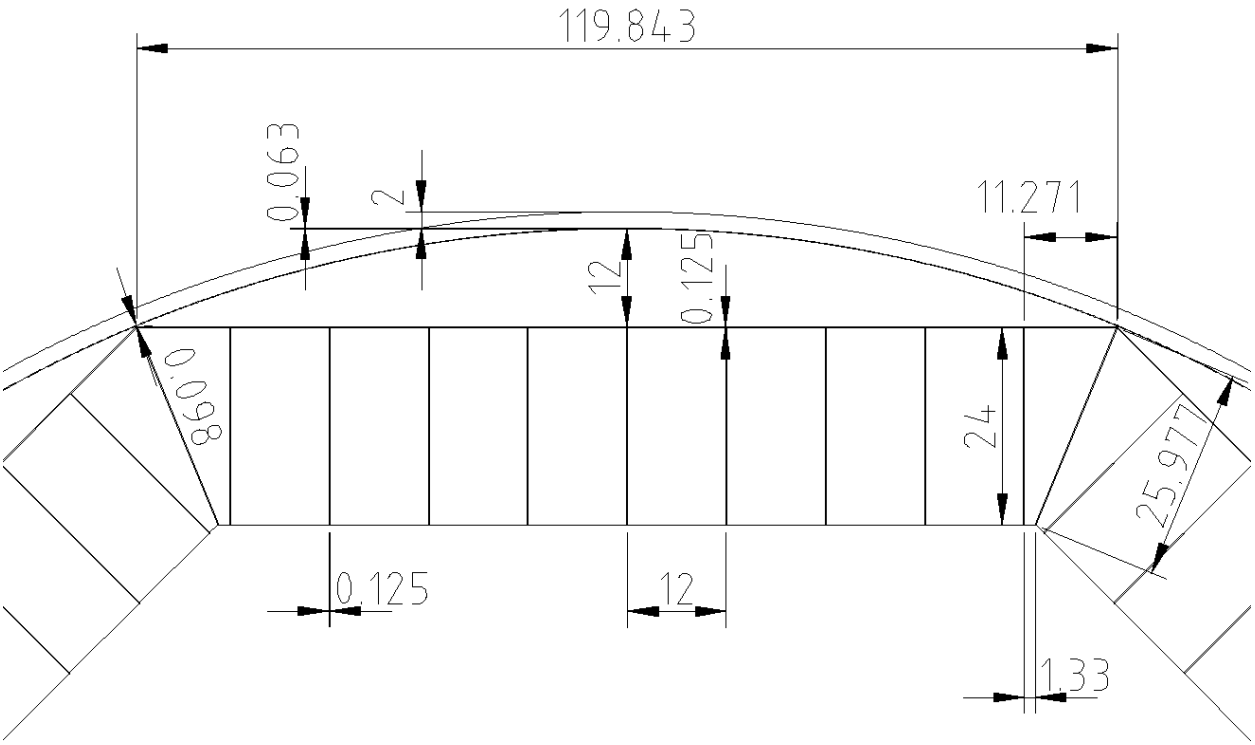

Figure 6. Approximate dimensions of inner and outer graphite reflector. Depiction is one of eight radial reflector sections, and the outer ring is the reactor vessel exterior wall. Dimensions are in inches.

The lower axial reflector is formed from concentric rings of graphite that are fixed to the lower reflector head on approximately 12 in. horizontal steps. The head has 1 in. holes, and the concentric ring has various spacing to permit a uniform flow velocity of ~7 fps and a pressure drop of ~5 psi across the holes and ~5 psi through the reflector. The upper reflector head is identical to the lower head with the exception that it has 6 additional holes to accommodate the control rods (Figure 7).

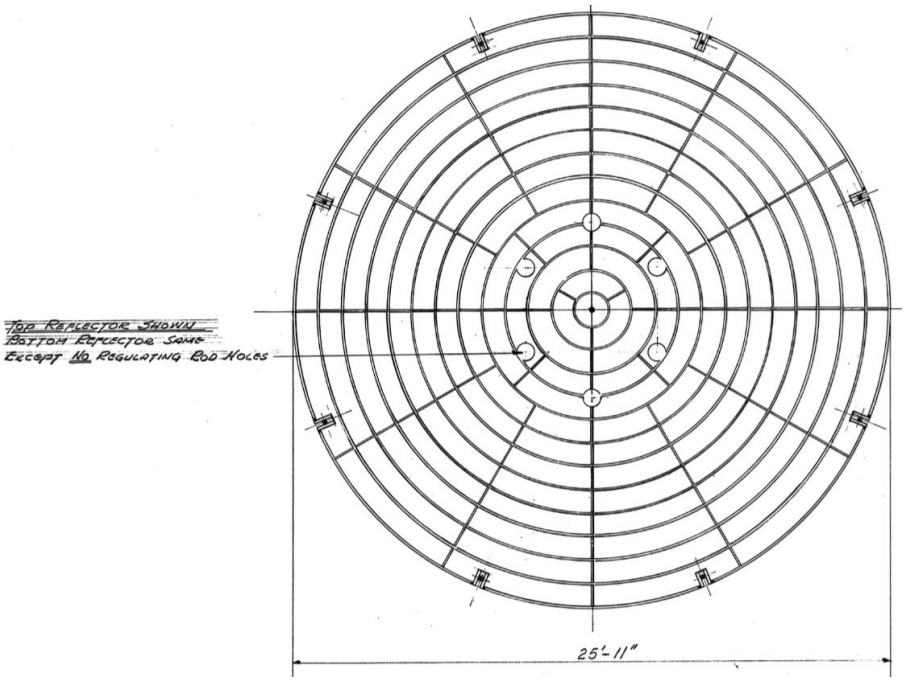

Figure 7. Top view of axial reflector showing concentric rings of graphite with narrow fluid channels between rings and between smaller graphite blocks within rings (Fig. 4 from Bettis, Alexander, and Watts 1972, ORNL DWG 72-4030).

The core of the reactor is filled with approximately 363 graphite cells. 357 of the cells are formed from an array of graphite slabs stacked in a square graphite matrix (Figure 8) with the fuel salt flowing through the gaps which are held at 0.142 in. using spacer dowels (black dots).

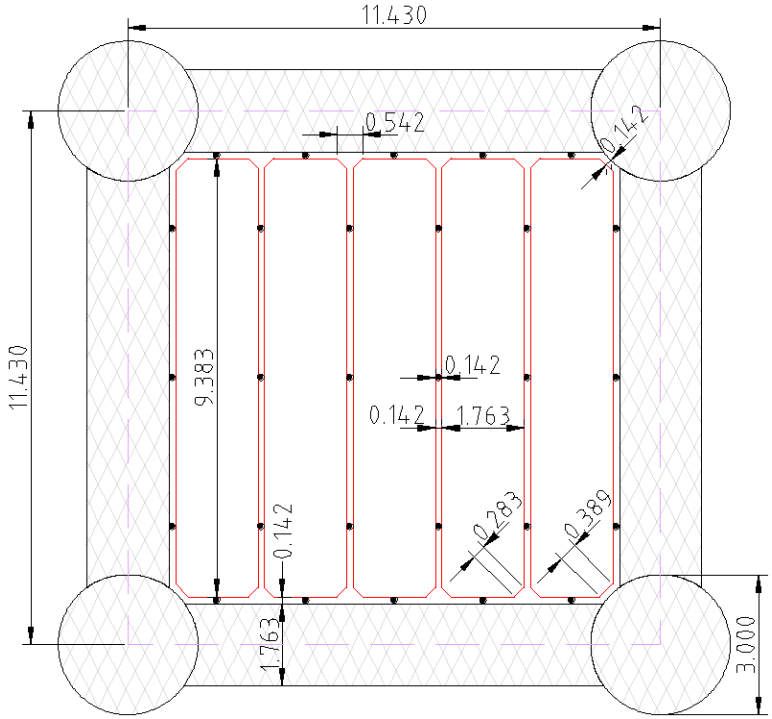

Figure 8. Reproduction of core cell (Fig. 7 from Bettis, Alexander, and Watts 1972, ORNL DWG 72-2830). Dimensions are in inches. The dashed magenta line indicates a unit cell.

The remaining six cells are sockets into which the six control rods are inserted (Figure 9).

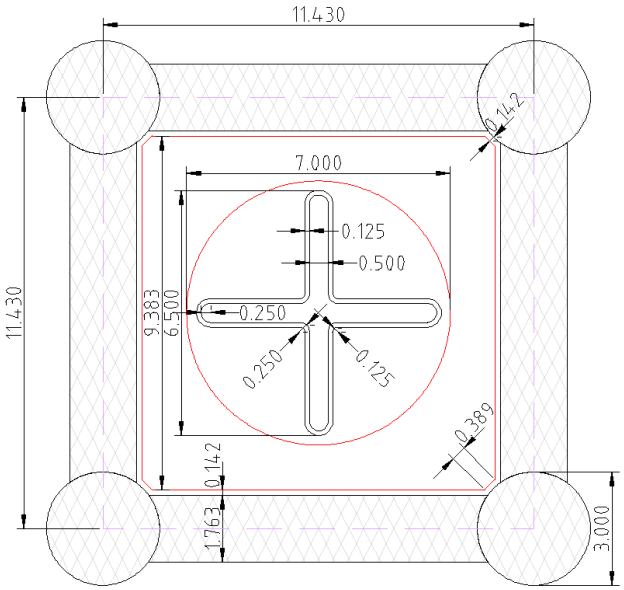

Figure 9. Reproduction of control rod cell (Fig. 12 A-A from Bettis, Alexander, and Watts 1972, ORNL DWG 72-3576) with the exterior graphite matrix added. Dimensions are in inches. The dashed magenta line indicates a unit cell.

An aerial view of the core and radial reflector with control rod locations is shown in Figure 10. The control rods are created from a slab of graphite of the same outer dimensions as the fuel cell and are bored with a 7 in. diameter hole and a 0.5 in. orifice at the bottom to permit salt to flow and cool the control rods. Each control rod is a 6.5 in. wide cruciform shape made of a 0.5 in. filler of boron carbide enclosed by 0.125 in. of Alloy-N, and each has a worth of 3%Δk/k in the original design. Fully inserted, the rods come within approximately 3 ft. of the bottom of the core. This gives an effective control rod length of 18 ft.

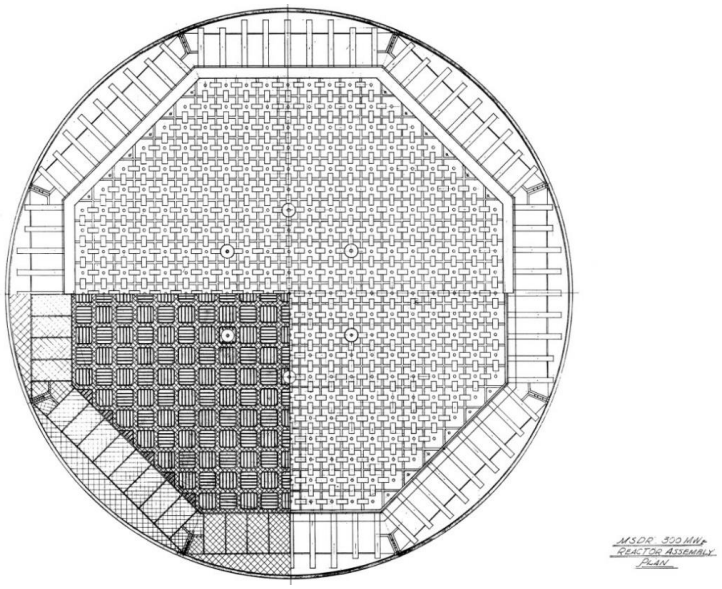

Figure 10. Reactor core and reflector plan (Fig. 6 from Bettis, Alexander, and Watts 1972, ORNL DWG 72-2826).

3.1.2 Fuel Pumps

The fuel pumps are sump-type centrifugal pumps (Figure 11) similar to those used in MSRE and are described in more detail in Robertson (Robertson 1971).

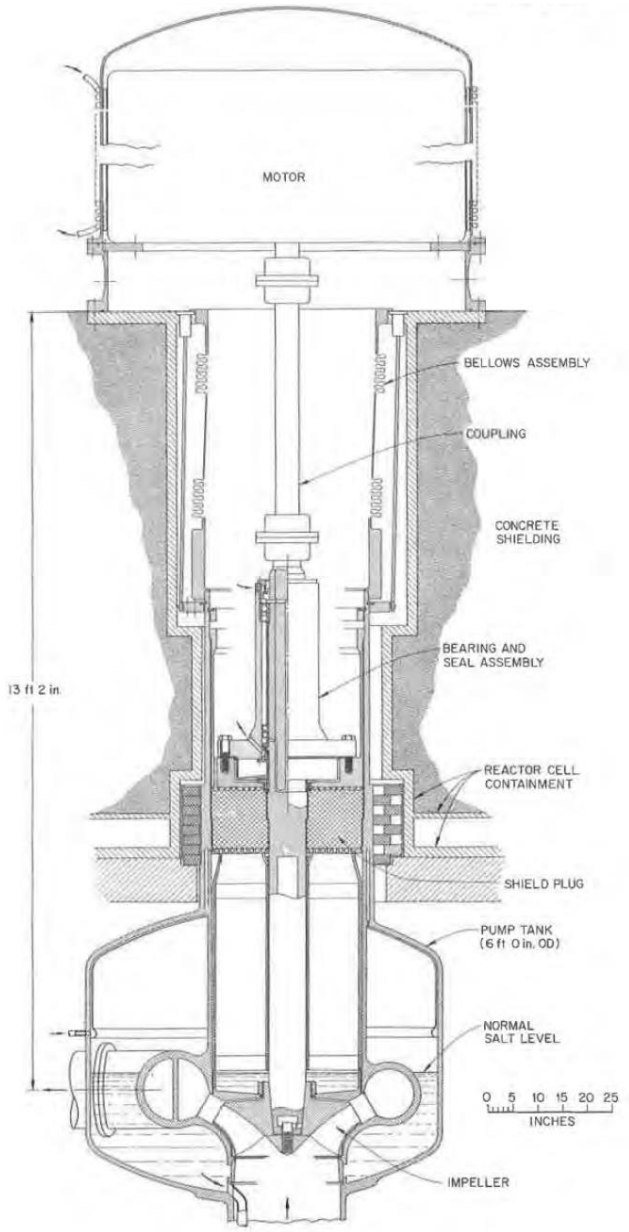

Figure 11. An example of a large sump-type fuel pump (Fig. 3.34 from Robertson 1971, ORNL DWG 96-6802).

The primary fuel loop has three pumps, each with a capacity of 8,100 gpm, and it develops a 150 ft. head mounted symmetrically on the top of the reactor vessel. Each pump is submerged in a tank with a large gas volume to accommodate salt expansion. The gas volume is connected to the center dome of the reactor vessel by a 6 in. overflow pipe. To purge fission gases from the salt, about 10% of the flow of each pump is bypassed directly from the pump outlet to the inlet. This bypass line contains a bubble generator and stripper which removes two volumes of salt for every volume of gas removed. The stripped gas and salt mixture is directed to the drain tank. Additional details of this bypass are discussed in later

sections. For this modeling activity, the detail of the pump used is limited to the size of the pump bowl, as initial models specify the mass flow rate. However, the flexibility of Modelica permits future models to include pumps of various levels of fidelity, including pump curves, gears, etc., to be created as necessary.

3.1.3 Primary Heat Exchangers

Each of the three fuel pumps supplies flow to two primary heat exchangers for a total of 6 heat exchangers. The MSDR design detailed a "U" type shell and tube heat exchanger. The expected operating conditions are still applicable and have been summarized in Table 1. These conditions are used in deriving the physical description of the heat exchangers employed in the dynamic model.

Table 1. Primary heat exchangers nominal operating conditions (Table 2 from Bettis, Alexander, and Watts 1972)

Parameter	Value	Unit
Number of heat exchangers	6	
Nominal capacity	125	MW/heat exchanger
Material	Alloy-N	
Tube-side conditions		
Fluid	Fuel salt	
Inlet/outlet temperature	1250 (677) / 1050 (566)	°F (°C)
Inlet pressure		psi (MPa)
Pressure drop	127 (0.876)	psi (MPa)
Mass flow rate	6.6e6 (832)	lb/hr (kg/s)
Shell-side conditions		
Fluid	Coolant Salt	
Inlet/outlet temperature	900 (482) / 1100 (593)	°F (°C)
Inlet pressure		psi (MPa)
Pressure drop	115 (0.793)	psi (MPa)
Mass flow rate	3.7e6 (466)	lb/hr (kg/s)

3.2 PRIMARY COOLANT LOOP

The primary coolant loop's principal purpose is to provide a buffer between the radioactive fuel salt and the balance of the power plant. Therefore, the loop is designed to hold a relatively small volume of salt. For this model, the primary coolant loop uses $^{7}LiF\text{-}BeF_2$, the same carrier salt as used in the primary fuel loop. There are three primary coolant loops, one for each fuel pump loop. Each loop has a sump-type pump similar to the primary fuel pump to account for thermal expansion and to circulate the flow through the two primary heat exchangers and the two secondary heat exchangers. The modeled design differs from the MSDR at this stage, as there is no secondary coolant loop. Instead, the primary coolant loop interacts directly with the power cycle. The nominal conditions defined for the secondary heat exchanger are summarized in Table 2. The primary restriction on the primary coolant loop and power cycle is to maintain conditions that will avoid freezing of the primary coolant (856 °F/ 458 °C). Given the importance of temperature control, this heat exchanger has many design and operational parallels to the steam generator discussed in Robertson (Robertson 1971).

Table 2. Secondary heat exchangers nominal operating conditions

Parameter	Value	Unit
Number of heat exchangers	6	
Nominal capacity	125	MW/heat exchanger
Material	Alloy-N	
Tube-side conditions		
Fluid	Supercritical Steam	
Inlet/outlet temperature	800 (427) / 1050 (566)	°F (°C)
Inlet pressure		psi (MPa)
Pressure drop	152 (1.048)	psi (MPa)
Mass flow rate	1.79e6 (225)	lb/hr (kg/s)
Shell-side conditions		
Fluid	Coolant Salt	
Inlet/outlet temperature	1100 (593) / 900 (482)	°F (°C)
Inlet pressure		psi (MPa)
Pressure drop	115 (0.793)	psi (MPa)
Mass flow rate	3.7e6 (466)	lb/hr (kg/s)

3.3 POWER CYCLE

The power cycle proposed for the MSDR was a conventional steam system operating at lower temperatures due to a secondary coolant loop with a nitrate-nitrate working fluid which was uncertain to perform at high temperatures (<1,000°F). The nitrate-nitrate secondary loop was primarily a means to limit migration of tritium to the environment. In the model for this report that secondary coolant loop has been removed and instead the primary coolant loop generates steam in the secondary heat exchanger. This creates the restriction on the power cycle such that it operates at a high temperature and pressure to prevent the primary coolant salt from freezing. Following the recommendations of Robertson (Robertson 1971), a supercritical steam Rankine cycle was selected as the power cycle for this dynamic model. The operating conditions in Table 2 are similar to those in Robertson (Robertson 1971) with the exception of the water side, which has a 100°F increase to the entrance temperature to account for the higher melting point of FLiBe (856°F) as compared to sodium fluoroborate (725°F) and a higher exit temperature and flowrate to offset the lower temperature differential permitted across the heat exchanger.

The overall power cycle converts thermal energy to electric power using once-through steam-generator superheaters, a turbine generator, and a regenerative feedwater heating system. The reference design is based on a much simplified version of that presented by Robertson (Robertson 1971) for the MSBR. The water leaves the secondary heat exchanger at 3,500 psia, 1050°F. A portion of the flow is sent to a preheater, which heats the exhaust of the high pressure (HP) turbine before being mixed with the feedwater and pumped back through the system. The main portion of flow from the secondary heat exchanger goes to the HP turbine, then to the preheater and reheater, and then to an intermediate pressure (IP) and low pressure (LP) turbine and condenser. The condensed fluid is then mixed with the diverted hot flow and pumped back through the secondary heat exchanger.

3.4 RESIDUAL HEAT REMOVAL SYSTEM

A drain tank below the reactor serves as the residual heat removal system and hold-up volume for the first stage of the fission product gas removed from the pump bowl. Fuel-salt in the drain tank gets pumped back to the primary fuel loop via a sump-pump style system. The drain tank vessel is approximately 11 ft. in diameter and 15 ft. tall. The vessel sits within a larger crucible for redundant containment (Figure 12), and the main connection to the primary fuel salt loop is via a 6 in. pipe and a freeze valve at the bottom of

the reactor vessel. The drain tank is penetrated by 60 double walled thimbles with NaK as the natural circulation coolant. The NaK coolant enters three tanks of water (25 × 25 × 12 ft. at ~60% full and at sufficient elevation above the drain tank to drive natural circulation) via double-walled tubes. As the drain tank is actively used for the off-gas system, it operates even under normal operation and not only during shutdown and accident scenarios. Nominal operating conditions of the drain tank are summarized in Table 3.

Table 3. NaK-water tank heat exchanger nominal operating conditions

Parameter	Value	Unit
NaK conditions		
Inlet/outlet temperature	532 (278) / 450 (232)	°F (°C)
Flow rate	2,800	gpm
Water Conditions		
Inlet/outlet temperature	80 (27) / 100 (212)	°F (°C)
Flow rate	39	gpm

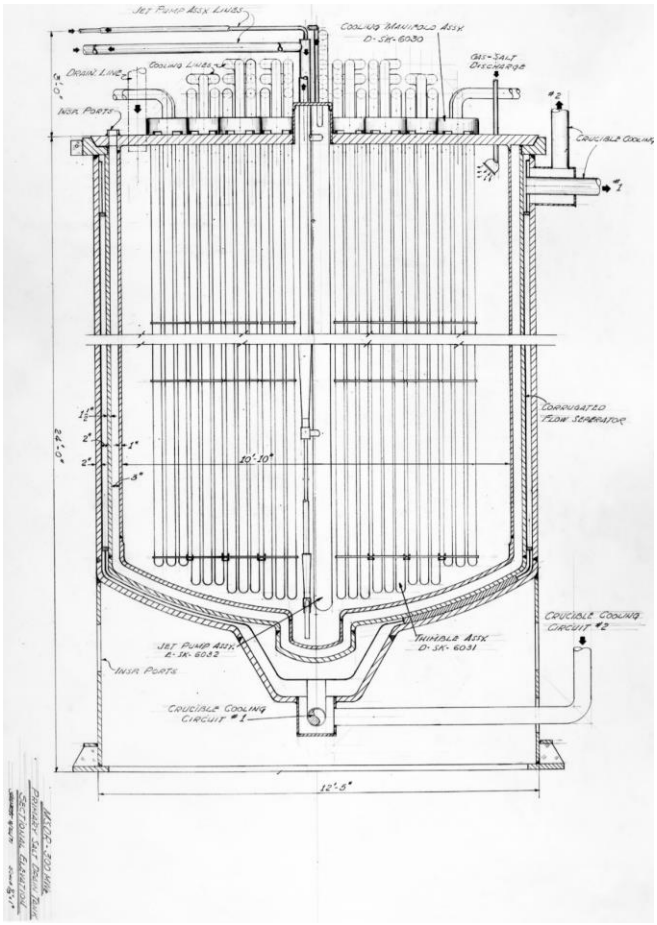

Figure 12. Drain tank (Fig. 21 from Bettis, Alexander, and Watts 1972).

3.5 OFF-GAS SYSTEM

Helium is used as the cover gas for the primary fuel and coolant salt and as the purge gas for removing fission products from the primary fuel salt. The off-gas from the pump with the mixed salt in a 2:1 salt-to-gas volume ratio goes to the drain tank where the gas separates from the salt. The salt is pumped back into the primary fuel loop. The buoyant forces separates the gas and is held up for approximately 6 hrs. before heading to one of two redundant particle traps. The particle traps remove the solid daughter products of the decaying gas and have NaK cooling designed for ~400 kW. After the particle traps, the gas line divides into two branches. One branch divides again and goes directly to the bubble generators in each of the three pump bypass lines. The other gas line enters one of two redundant charcoal absorber beds. The charcoal bed provides a 90-day hold-up of the gas before going to a gas compressor and storage tank. The 90-day charcoal bed is cooled by natural circulation with air and NaK cooling. The gas in the storage tank is then used for recirculation to the pump seals and is therefore reintroduced into the primary fuel salt.

3.6 CONCEPT DESCRIPTION SUMMARY

The historical reports of the MSDR and MSBR provides sufficient information for many aspects of an MSR concept, especially for a generic system level model. In particular, geometry and heat exchanger information was valuable in obtaining a rough estimate of the amount of salt and graphite are in the primary fuel loop. However, information which governs much of the behavior of the reactor such as pump curves and reactor kinetic information (e.g., feedback coefficients and effective delayed neutron fractions) were omitted along with minimal details surrounding auxiliary systems (e.g., charcoal bed system). Where necessary engineering judgement, best-guess estimates, or simplifying assumptions were made in the implementation of the dynamic model as discussed in the following section.

4. DYNAMIC MODEL

The following section describes the dynamic model created using the open-source ORNL-developed Modelica library TRANSFORM (Greenwood et al. 2017). Readers are directed to the TRANSFORM library for additional details regarding components, methods, assumptions, etc. not covered in this report.

The fluoride salt-fueled, thermal reactor dynamic model is shown in Figure 13 and Figure 14. The model follows the general design requirement described in Section 3. The subsequent subsections identify the key assumptions made for each loop and provide other pertinent information for understanding the model implementation. In general, cross sectional flow areas, wetted perimeters, surface areas, and volumes were attempted to be conserved to provide reasonable representations of the more complex system. Summaries of the overall mass and volumes of graphite and salts, components, and parameters are presented in Table 4 through Table 8.

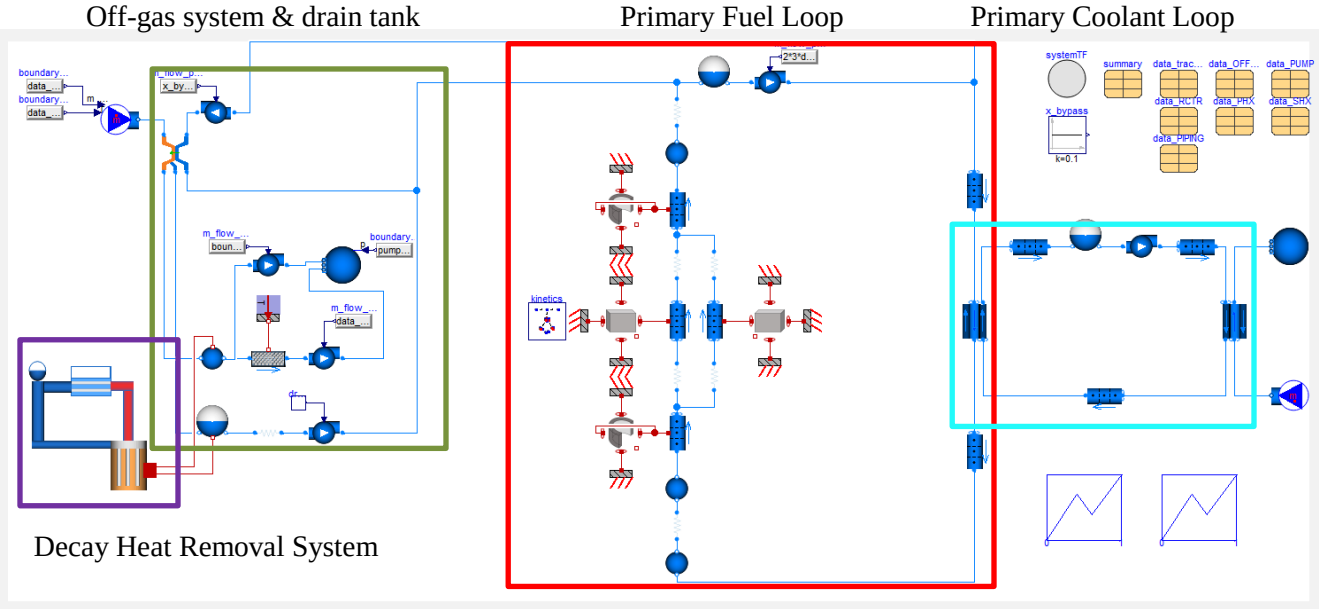

Figure 13. Dynamic model of the fluoride–salt-fueled, thermal reactor based.

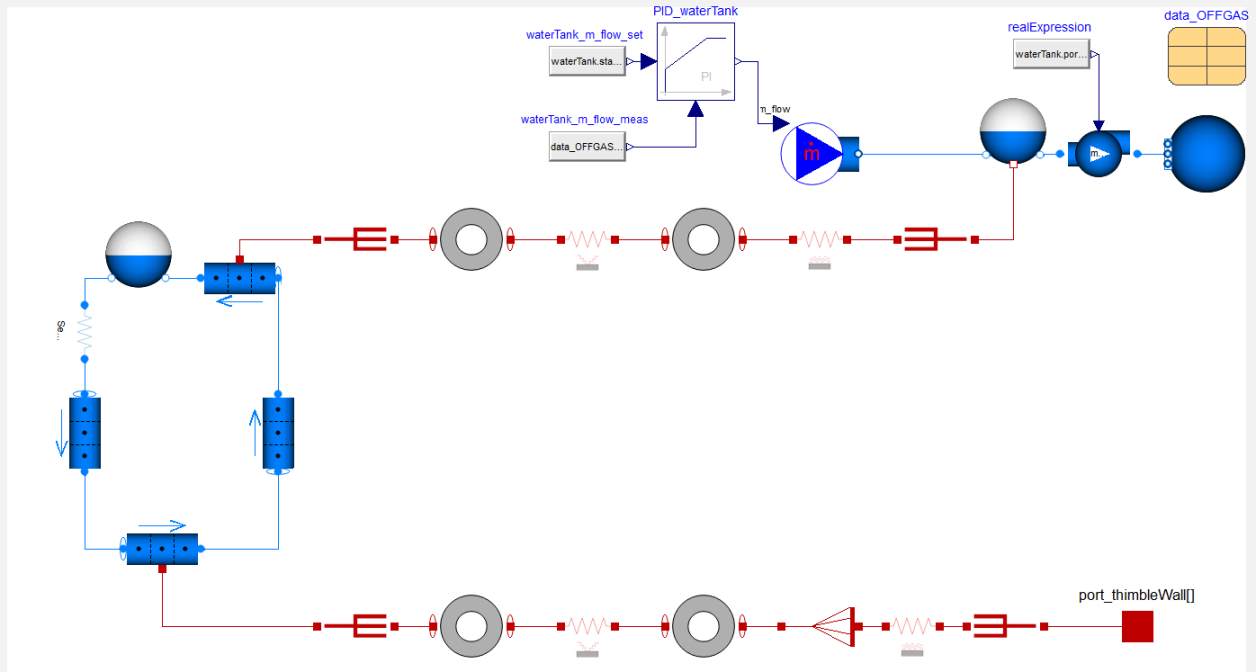

Figure 14. Dynamic model of the drain tank natural circulation decay heat removal system.

Table 4. Summary of mass and volumes of graphite and salt in the primary fuel and coolant loops

Component	Parameter	Value	Unit
Reactor summary	Total mass of graphite	662436.4	kg
	Total mass of salt	100802.38	kg
	Total volume of graphite	372.8544	m^3
	Total volume of salt	30.0604	m^3
	Mass fraction of salt	0.132	-
	Volume fraction of salt	0.075	-
Primary flow loop	Total mass of salt	138541.36	kg
	Total volume of salt	41.312423	m^3
Primary coolant loop	Total mass of salt	87758.976	kg
	Total volume of salt	43.376688	m^3
Reference values for volume calculation:			
Primary flow loop	Temperature	625	°C
	Pressure	1	bar
	Graphite density	1776.66	kg/m^3
	Salt density	3353.33	kg/m^3
Primary coolant loop	Temperature	525	°C
	Pressure	1	bar

Table 5. Summary of reactor components

Component	Parameter	Value	Unit
Per axial reflector	Number of characteristic graphite blocks	123.334	-
	Graphite block dimensions (R_{in}, R_{out}, H)	1.52216, 1.82014, 1.2192	m
	Swept angle for graphite block	29.8085	°
	Total cross sectional flow area	0.671261	m^2
	Total wetted perimeter	393.135	m
	Heat transfer coefficient	22372.1	W/(m-K)
	Total fluid-graphite surface area	261.471	m^2
	Total mass of graphite	69212.7	kg
	Total mass of salt	2716.89	kg
	Total volume of graphite	38.9567	m^3
	Total volume of salt	0.810205	m^3
	Mass fraction of salt	0.037772	-
	Volume fraction of salt	0.020374	-
Radial reflector	Number of characteristic graphite blocks	199.283	-
	Graphite block dimensions (L, W, H)	0.1524, 0.6096, 6.4008	m
	Total cross sectional flow area	0.269823	m^2
	Total wetted perimeter	191.866	m
	Heat transfer coefficient	1006.09	W/(m-K)
	Total fluid-graphite surface area	777.587	m^2
	Total mass of graphite	210542	kg
	Total mass of salt	5862.4	kg
	Total volume of graphite	118.504	m^3
	Total volume of salt	1.74823	m^3
	Mass fraction of salt	0.02709	-
	Volume fraction of salt	0.014538	-
Core	Nominal thermal power	750	MWt
	Number of characteristic graphite blocks	4998	-
	Graphite block dimensions (L, W, H)	0.0223901, 0.246322, 6.4008	m
	Total cross sectional flow area	2.4234	m^2
	Total wetted perimeter	1444.77	m
	Heat transfer coefficient	843.515	W/(m-K)
	Total fluid-graphite surface area	7880.15	m^2
	Total mass of graphite	313469	kg
	Total mass of salt	52073.8	kg
	Total volume of graphite	176.437	m^3
	Total volume of salt	15.529	m^3
	Mass fraction of salt	0.142456	-
	Volume fraction of salt	0.080895	-
Per reactor plenum	Total mass of salt	18716.2	kg
	Total volume of salt	5.58138	m^3
Reactor inlet tee	Total mass of salt	1438.53	kg
	Total volume of salt	0.426847	m^3

Table 6. Summary of primary fuel loop components (excluding reactor)

Component	Parameter	Value	Unit
Primary heat exchanger loop	Number of loops	3	
Pump bowl (per loop)	Diameter	1.2192	m
	Height	1.2192	m
	Nominal level	0.6096	m
	Total mass of salt	2361.8	kg
	Total volume of salt	0.704313	m^3
Pipe to PHX (per loop)	Diameter	0.3048	m
	Length	6.096	m
	Total mass of salt	1476.62	kg
	Total volume of salt	0.440345	m^3
Pipe to PHX (per loop)	Diameter	0.3048	m
	Length	17.3736	m
	Total mass of salt	4303.01	kg
	Total volume of salt	1.2832	m^3
Primary heat exchanger (per loop)	Number of heat exchangers	2	
	Nominal capacity per heat exchanger	125	MW
Tube-side conditions (nominal)	Working fluid	Fuel Salt	-
	Inlet temperature	676.667	°C
	Outlet temperature	565.556	°C
	Inlet pressure	12.4106	bar
	Static pressure drop	11.4131	bar
	Mass flow rate	831.585	kg/s
Shell-side conditions (nominal)	Working fluid	Coolant Salt	-
	Inlet temperature	482.222	°C
	Outlet temperature	593.333	°C
	Inlet pressure	10.2732	bar
	Static pressure drop	9.27269	bar
	Mass flow rate	466.192	kg/s
Tube side	Tube material	Alloy-N	-
	Number of tubes	1368	-
	Tube outer diameter	0.009525	m
	Tube thickness	0.000889	m
	Tube length	9.144	m
	Tube pitch (triangular)	0.0170688	m
	Heat transfer coefficient	14985.4	W/(m-K)
	Total surface area	304.443	m^2
	Total mass of salt	1979.36	kg
	Total volume of salt	0.590267	m^3
Shell side	Total cross sectional flow area	0.25354	m2
	Total wetted perimeter	43.0358	m
	Heat transfer coefficient	27302.9	W/(m-K)
	Total surface area	374.315	m^2
	Total mass of salt	4677.15	kg
	Total volume of salt	2.31178	m^3

Table 7. Summary of primary coolant loop components (excluding primary heat exchanger)

Component	Parameter	Value	Unit
Primary coolant loop	Number of loops	3	
Pump bowl (per loop)	Diameter	1.2192	m
	Height	1.2192	m
	Nominal level	0.6096	m
	Total mass of salt	1454.73	kg
	Total volume of salt	0.719029	m^3
Pipe to PHX to pump bowl (per loop)	Diameter	0.3048	m
	Length	4.572	m
	Total mass of salt	663.981	kg
	Total volume of salt	0.328186	m^3
Pipe to pump bowl to SHX (per loop)	Diameter	0.3048	m
	Length	2.4384	m
	Total mass of salt	354.123	kg
	Total volume of salt	0.175033	m^3
Pipe SHX to PHX (per loop)	Diameter	0.3048	m
	Length	6.4008	m
	Total mass of salt	954.918	kg
	Total volume of salt	0.471988	m^3
Secondary heat exchanger (per loop)	Number of heat exchangers	2	
	Nominal capacity per heat exchanger	125	MW
Tube-side conditions (nominal)	Working fluid	Supercritical water	-
	Inlet temperature	426.667	°C
	Outlet temperature	565.556	°C
	Inlet pressure	258.691	bar
	Static pressure drop	10.48	bar
	Mass flow rate	225.536	kg/s
Shell-side conditions (nominal)	Working fluid	Coolant salt	-
	Inlet temperature	593.333	°C
	Outlet temperature	482.222	°C
	Inlet pressure	18.2022	bar
	Static pressure drop	9.27369	bar
	Mass flow rate	466.192	kg/s
Tube side	Tube material	Alloy-N	-
	Number of tubes	1604	-
	Tube outer diameter	0.009525	m
	Tube thickness	0.000889	m
	Tube length	11.43	m
	Tube pitch (triangular)	0.0182575	m
	Heat transfer coefficient	17594.1	W/(m-K)
	Total surface area	446.205	m^2
	Total mass of water	85.8181	kg
	Total volume of water	0.907746	m^3
Shell side	Total cross sectional flow area	0.35707	m^2
	Total wetted perimeter	50.4314	m
	Heat transfer coefficient	23569.7	W/(m-K)
	Total surface area	548.612	m^2
	Total mass of salt	8235.47	kg
	Total volume of salt	4.07055	m^3

Table 8. Summary of off-gas and decay heat removal system components

Component	Parameter	Value	Unit
Fuel salt pump bypass line	Fraction of mass flow	0.1	-
	Mass flow rate	554.39	
Off-gas separator	Volumetric flow rate	9.464	m^3/s
	Volumetric ratio of salt removed to gas flow	2.0	
	Substance removal efficiency	1.0	
	Substances separated	Gaseous fission products	-
Charcoal bed	Fraction of gas to bed	0.5	-
	Characteristic delay time	90	day
	Basis for characteristic time	Xe	-
Drain tank	Salt inlet mass flow rate	6.28	
	Salt outlet mass flow rate	Control dependent	
	Cross sectional area (excludes internal piping)	6.92	m^2
	Height	5.334	m^2
Decay heat removal design references	Hot nak temperature	278	°C
	Cold nak temperature	232	°C
	Inlet water temperature	27	°C
	Outlet water temperature	38	°C
	Nak mass flow rate	142	kg/s
	Water mass flow rate	2.45	kg/s
Decay heat removal system	Type	Double-walled	-
	Material	Alloy-N	-
	Working fluid	NaK	-
	Number of thimbles in drain tank	360	-
	Number of water tanks	3	-
	Number of thimbles per water tank	576	-
	Dimensions of each water tank (l, w, h)	7.62, 7.62, 3.66	m
	Nominal level of water tank	1.83	m
	Outer thimble pipe diameter (3-in. Sch-10)	8.89	cm
	Outer thimble pipe thickness	0.305	cm
	Inner thimble pipe diameter (3-in. Sch-10)	6.03	cm
	Inner thimble pipe thickness	0.391	cm
	Drain tank thimble length	5.33	m
	Water tank thimble length	7.62	m
	Elevation change between tanks	18.3	m

4.1 PRIMARY FUEL LOOP

The primary fuel loop (PFL) is defined as the primary circuit of fuel salt, which includes the reactor, primary fuel pump, piping to and from the primary heat exchanger, and the primary heat exchanger (fuel side). Each component is modeled and hydraulically connected and or thermally connected as shown in Figure 13. The dimensions and relevant parameters of each of the components are summarized in Table 5 and Table 6.

The principal component of the PFL is the reactor. The reactor consists of an inlet and outlet plenum and axial reflectors, a radial reflector, and the core. The inlet and outlet plenums are ideally mixed volumes and are identical. The inlet and outlet graphite reflectors are identical and are made from radial rings of graphite with each ring consisting of several smaller sections of graphite. To generalize the geometry, a

graphite block of the 6th ring was chosen as the representative geometry of the solid portion of the subchannel (Figure 15), and the number of identical blocks was scaled to conserve the overall volume of graphite. The solid model was then implemented as a 2D radial (r-z) conduction model with the specified number of parallel graphite blocks. Heat and mass transfer are modeled on the inner and outer radial surface and neglected on the top, bottom, and short edge. The fluid subchannel is represented by a 1D discretized homogeneous fluid with geometry specified by the total cross sectional area and wetted perimeter of the reflector.

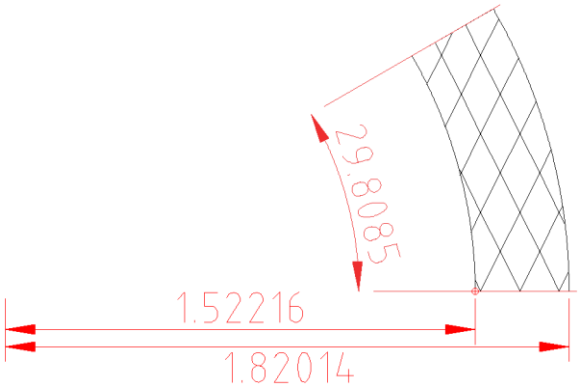

Figure 15. Characteristic geometry of the graphite blocks of the axial reflectors

The radial reflector is similarly modeled as the axial reflectors, except the solid model is a 2D slab (x-z) conduction model where the characteristic block is identical to the vertical rectangular blocks show in Figure 6. Additionally, the slab is assumed to have an adiabatic centerline which permits modeling only half of the slab by increasing the number of parallel characteristic solids by a factor of two. Heat and mass transfer are neglected on the top, bottom, and small edge of the block.

The core region solid is modeled like the radial reflector but with characteristic dimensions the same as the individual center graphite block in a fuel cell (Figure 8) except slightly longer to conserve graphite volume. The fluid channel is determined by the cross sectional flow area and wetted perimeter of the model.

The piping to and from the primary fuel heat exchanger dimensions are approximated based on rough estimations from drawings as they were not specified in available documentation. Likewise, the pump and pump bowl were never fully defined. Therefore, the dimensions of the pump bowl were assumed to be on the order of the MSBR, though slightly smaller, and the pump is ideal, producing the specified flow rate. The off-gas system interfaces with the primary loop at the pump bowl inlet and pump outlet by cycling a fraction of the overall flow through a separator to strip fission product gas products and then returns to the pump bowl. A small amount of fuel salt also leaves the system and travels to the drain tank, where it is then pumped back to the pump bowl. The amount of salt sent to the drain tank and back to the pump bowl depends on the flow rate of carrier gas for the off-gas system and the level controls of the drain tank pumping system. Additional information on the off-gas and drain tank systems is detailed in a later section.

The primary fuel heat exchanger is a simple shell-and-tube heat exchanger with the dimensions specified in Bettis et al. (Bettis, Alexander, and Watts 1972). Secondary aspects of the heat exchanger (e.g., inlet/outlet volumes and resistances) are not included. Tritium is permitted to flow through the heat exchanger tube walls to the primary coolant loop (Mays, Smith, and Engel 1977). The modeling approach is discussed in detail in Rader and Greenwood (Rader and Greenwood 2018).

Substances such as neutron precursor groups and fission products are treated as trace substances which are transported at a rate equal to the primary carrier fluid. As appropriate, the decay of products, heat deposition, chemical relation, etc. are also included in each volume.

4.1.1 Trace Substances

A trace substance is assumed to be in very small quantities, so it has an insignificant impact on the mass of the system. The trace substance is tracked as an unspecified mass weighted fraction of the primary flow. This means that the trace substance flows as a homogenous part of the primary fluid, but it does not participate in the normal mass balance of the primary fluid, and the absolute units of the traced substance are inconsequential. For example, if the primary fluid flows at 1 kg/s and a trace substance (C) mass weighted fraction is 100 atoms C/kg fluid, then the primary fluid mass balance assumes there is 1 kg/s of primary fluid, and the trace substance mass has its own "mass" balance tracking the 100 atoms/s flowing through the system. This method allows for mapping of small quantities of substances on traditional thermal-hydraulic processes as a first-order approximation, obviating the need to create complex media proprieties, pressure loss functions, etc. Although the trace substance methodology does not specify a particular unit, if the modeler uses the substance concentrations for other calculations (e.g., diffusion across a phase boundary), then the appropriate unit conversions must be applied (e.g., convert from atoms to moles using molecular weight and Avogadro's number).

4.2 PRIMARY COOLANT LOOP

The primary coolant loop is defined as the primary circuit of coolant salt, which includes the primary heat exchanger (coolant side), coolant pump, secondary heat exchanger (coolant side), and associated piping. Each of these components is modeled and hydraulically or thermally connected as shown in Figure 13. The dimensions and relevant parameters of the components are summarized in Table 7. The primary heat exchanger portion is included in Table 6.

Apart from the coolant, tritium is transported through the primary coolant loop as a trace substance. It enters the loop from the primary heat exchanger and leaves through the secondary heat exchanger.

4.3 POWER CYCLE BALANCE OF PLANT

The preliminary model uses boundary conditions of outlet pressure, inlet flow rate, and enthalpy consistent with a supercritical water cycle as presented in the concept description. Detailed power cycles, including turbines, reheaters, etc., can be readily incorporated into future system models in lieu of boundary conditions to investigate the steady-state and transient behavior of a complete system model.

4.4 OFF-GAS SYSTEM, DRAIN TANK, AND DECAY HEAT REMOVAL SYSTEM

The interrelated off-gas, drain tank, and decay heat removal systems are presented together. A summary of each system and its components is presented in Table 8 and discussed below. In general, these systems were underdefined to varying degrees in literature, so engineering judgment and simplifications were made for preliminary modeling purposes.

4.4.1 Off-Gas System

The off-gas system removes a specified set of trace substances from the primary fuel salt pump bypass line at a specified efficiency using a helium carrier gas. A portion of primary fuel salt is also carried from the primary fuel loop with a rate dependent on the carrier gas flow rate. The separated fuel salt travels directly to the drain tank, where is then pumped back to the pump bowl of the primary fuel loop. The rate

of fuel salt return from the drain tank is a controllable parameter based on the control settings of the drain tank sump pump. The carrier gas with the separated trace substances also travels to the drain tank. The characteristic hold-up time of the gas is dependent on the volume of the tank. From the drain tank, the gas is split at a specified ratio between a return line directly back to the pump bowl and a charcoal adsorber bed. As the gas passes through the charcoal bed, substances decay, give off heat, and are potentially trapped. After exiting the charcoal bed, the carrier gas and any remaining substances that did not completely decay or were otherwise filtered are then returned to the pump bowl.

The charcoal bed transports (Sun et al. 1994) the trace substances between volumes in the adsorber bed at a rate ($m\dot{C}$) which is a function of the inflow rate, the time spent in a volume (τ), the decay rate of the substance (λ), and any sources of each substance from the decay of other substances, as shown in the following equation:

$$m\dot{C}_{out} = m\dot{C}_{in}e^{-\lambda\tau} + \sum m\dot{C}_{decay}$$

The adsorber bed is heated by the associated decay of substances. The adsorber bed is cooled by a passive circulation loop like the drain tank heat removal system. However, for simplicity, a fixed boundary temperature is set for the adsorber bed where the cooling requirement can be simply monitored, as no design information is available for that system.

4.4.2 Drain Tank

The drain tank is separated into two volumes, one for the gas and one for the fuel salt. The gas volume is determined by the liquid level of the fuel salt in the specified geometry, while the pressure of the fuel salt volume is set by the gas volume. Products decay and give off heat in each of these volumes and then continue through the process. The gas volume continues to the adsorber bed or directly to the pump bowl as previously discussed, while the fuel salt is pumped back to the pump bowl based on the control algorithm implemented. The default control keeps the salt level constant by pumping salt back to the pump bowl at the same rate as which salt enters the drain tank. The drain tank is thermally connected with the decay heat removal system through double-walled thimbles as described below.

4.4.3 Decay Heat Removal

The decay heat removal system is a passive, buoyance-driven, NaK-filled circulation loop. The loop removes heat from the drain tank via double-walled thimbles which rely on radiation heat transfer between the pipes and convective heat transfer between the working fluids and the pipe walls. The hot fluid rejects to a water tank at a higher elevation via identical double-walled thimbles. The cold fluid recirculates back to the drain tank to then be reheated. As this system is not well defined, a flow resistance is inserted into the loop so that the mass flow rate matches the design references. This resistance would be comprised of bends, orifices, and other pressure losses not already accounted for by the pressure drop correlations in the pipes. The water tank has a simple control system that keeps the outlet temperature at the design condition. The current model of the water tank is a simple, ideally mixed volume that does not consider latent heat effects, so this results in an overestimation of the amount of flow required to keep the tank at design conditions.

4.5 MEDIA THERMOPHYSICAL PROPERTIES

4.5.1 Fuel Salt

The primary fuel loop fluid is a linear compressible FliBe using fueled salt properties. This extends from the “PartialLinearFluid” interface from the Modelica Standard Library (Modelica Association [2013]

2018). The linear compressible fluid model indicates that the density is a linear function of temperature and pressure and assumes the following:

- The specific heat capacity at constant pressure (cp) is constant
- The isobaric expansion coefficient (beta) is constant
- The isothermal compressibility (kappa) is constant
- Pressure and temperature are used as states
- The influence of density on specific enthalpy (h), entropy (s), inner energy (u) and heat capacity (cv) at constant volume is neglected.

The inputs to the model are tabulated in Table 9. These parameters are taken from Bettis et al. (Bettis et al. 1972) or modified (beta/kappa) to match the temperature dependence of density using a reference temperature of 800 K.

Table 9. Specified thermophysical properties of a linear compressible implementation of fueled FLiBe (Temperature in K)

Parameter	Value	Unit
Composition	LiF-BeF_2-ThF_4-UF_4 71.5%-16%-12%-0.5%	Mole %
Constant pressure heat capacity	1,340	J/(kg-K)
Thermal conductivity	1.3	W/(m^2-K)
Dynamic viscosity	$1.09 \cdot 10^{-4} e^{4090/T}$	kg/(s-m)
Isobaric expansion coefficient	1.964787e-4	1/K
Isothermal compressibility	2.89e-10	1/Pa

4.5.2 Coolant Salt

The primary coolant loop fluid is a linear compressible FLiBe which extends from the same interface as the fuel salt and has the same assumptions as the fuel salt. The inputs to the model are tabulated in Table 10 using a reference temperature of 800 K. These parameters are taken from Bettis et al. (Bettis et al. 1972)

Table 10. Specified thermophysical properties of a linear compressible implementation of FLiBe (Temperature in K)

Parameter	Value	Unit
Composition	LiF-BeF_2 67%-33% (99.99% ^{7}Li)	Mole %
Constant pressure heat capacity	2416	J/(kg-K)
Thermal conductivity	$0.0005T + 0.63$	W/(m^2-K)
Dynamic viscosity	$1.16 \cdot 10^{-4} e^{3755/T}$	kg/(s-m)
Isobaric expansion coefficient	2.14151e-4	1/K
Isothermal compressibility	2.89e-10	1/Pa

4.5.3 Decay Heat Removal System Salt

The decay heat removal system fluid is a linear compressible NaK which extends from the same interface as the fuel salt and has the same assumptions as the fuel salt. The inputs to the model are tabulated in Table 11 with fitting data taken from (Kirillov 2006) using a reference temperature of 550 K.

Table 11. Specified thermophysical properties of a linear compressible implementation of FLiBe (Temperature in K)

Parameter	Value	Unit
Composition	NaK 22%-78%	Mole %
Constant pressure heat capacity	893	J/(kg-K)
Thermal conductivity	$15 + 30.29 \cdot 10^{-3} T - 20.81 \cdot 10^{-6} T^2$	W/(m^2-K)
Dynamic Viscosity	$9.3083 \cdot 10^{-5} e^{556/T}$	kg/(s-m)
Isobaric expansion coefficient	3.0286e-4	1/K
Isothermal compressibility	2.89e-10	1/Pa

4.5.4 Power System Balance of Plant

The power system balance of plant fluid is a Modelica implementation of the IAPWS/IF97 standard which is a part of the Modelica Standard Library (Modelica Association [2013] 2018).

4.5.5 Graphite

The graphite for all regions of the core are based on a solid media implementation that permits the modeler to specify functional relations of thermophysical properties as a function of temperature. The default graphite is unirradiated nuclear graphite with the properties specified in Table 12.

Table 12. Specified thermophysical properties of primary fuel loop graphite (Temperature in K)

Parameter	Value	Unit
Specific heat capacity	$-144 + 3.67T - 2.2e^{-3}T^2 + 4.63e^{-7}T^3$	J/(kg-K)
Thermal conductivity	$169 - 0.125T + 3.28e^{-5}T^2$	W/(m^2-K)
Density	1776.66	kg/m^3

4.5.6 Alloy-N

The vessel and piping material (including heat exchangers) for the primary fuel and coolant loop are based on a solid media implementation that permits the modeler to specify functional relations of thermophysical properties as a function of temperature. The default material is alloy-N with the properties specified in Table 13.

Table 13. Specified thermophysical properties of Alloy-N (Temperature in K)

Parameter	Value	Unit
Specific heat capacity	$489 - 0.34T + 4.6e^{-4}T^2$	J/(kg-K)
Thermal conductivity	$9.77 - 3.2e - 4T + 1.46e^{-5}T^2$	W/(m^2-K)
Density	8,860	kg/m^3

4.5.7 Carbon Adsorber Bed

Estimated charcoal bed properties are shown in Table 14 (Fuderer 1985).

Table 14. Specified thermophysical properties of charcoal adsorber bed

Parameter	Value	Unit
Specific heat capacity	1,256	J/(kg-K)
Density	481	kg/m^3

4.6 PRESSURE LOSS AND HEAT & MASS TRANSFER CORRELATIONS

4.6.1 Pressure Loss

The pressure loss of flow through pipes is calculated based on the common Swamee and Jain correlation for the turbulent region and circular pipe for laminar (Table 15). The implementation is based on a modified implementation of the "DynamicPipe" component from the Modelica Standard Library which includes flow reversal, static head, and momentum losses. Other minor losses through the system are ignored unless specified.

Table 15. Frictional pressure loss correlations for pipes

Turbulent – Swamee and Jain	$\frac{1}{\sqrt{f}} = -2\log\left(\frac{\epsilon}{3.7D_h} + \frac{2.51}{Re\sqrt{f}}\right)$
Laminar – circular Pipe	$f = 64/\mathrm{Re}$

4.6.2 Heat Correlations

The heat transfer correlations for all single-phase fluids under turbulent conditions uses the Dittus-Boelter equation. Laminar conditions use the solution for circular pipes (Table 16) ($Nu = \alpha L/\lambda$). There is significant uncertainty in the appropriateness of these correlations, although they do appear to be reasonable approximations given the vast number of uncertainties associated with these advanced systems (Yoder 2014). Radiative heat transfer is not currently modeled unless otherwise specified (i.e., decay heat removal system double walled thimbles) but may be added as part of future work.

Table 16. Heat transfer correlations for pipes

Turbulent – Dittus-Boelter	$\mathrm{Nu} = 0.023 * \mathrm{Re}^{0.8}\mathrm{Pr}^{0.4}$
Laminar – circular pipe	$\mathrm{Nu} = 4.36$

4.6.3 Mass Transfer Correlations

In this preliminary model, tritium was of primary consideration for mass transfer to graphite surfaces and diffusion through the primary and secondary heat exchangers. For this model, all tritium atoms were considered to be T_2. An additional relation of TF and T_2 must be specified as T_2, which is the diffusive species. Therefore, this assumption yields a greater diffusive potential than would otherwise be expected given the model's parameters.

The diffusion of tritium to surfaces, whether graphite or metal, followed a mass transfer analogy using a Sherwood number in a laminar or turbulent region ($Sh = \alpha_m L/D_{ab}$). Parameters are taken from (Stempien 2015). The diffusion coefficient of the tritium in FLiBe was taken as the Arrhenius expression below with the appropriate properties specified in Table 17.

$$D_{ab} = D_{ab0}e^{-E_a/RT}$$

Table 17. Arrhenius parameters for tritium diffusion

Parameter	FLiBe	Alloy-N	Graphite
D_{ab0} [m^2/s]	9.3e-7	7.43e-7	9e-5
E_a [J/mol]	4.2e4	4.41e4	2.7e5

Table 18. Mass transfer to surfaces correlations for tritium.

Turbulent – Dittus-Boelter	$\mathrm{Sh} = 0.023 * \mathrm{Sc}^{0.8}\mathrm{Pr}^{0.4}$
Laminar – Sieder-Tate	$\mathrm{Sh} = 1.86 Re^{1/3} Sc^{1/3} \left(\frac{D}{L}\right)^{1/3}$

The interface condition between the salt and the solid surface requires the introduction of a Henry and Sieverts law condition to describe the solubility of the tritium gas in each of the substances. This is important, as it accounts for the discontinuous concentration at the interface that permits tritium flow direction to be driven by a concentration gradient due to the behavior of solubility. The equation for this interface condition is given below. The solubility coefficient (k) is calculated from an Arrhenius expression in the solid (k_S) and an exponential expression in the fluid (k_H).

$$\frac{C_{salt}}{k_H} = \left(\frac{C_{solid}}{k_S}\right)^2$$

$$k_H = k_0 e^{-BT}$$

$$k_S = k_0 e^{-\Delta H/RT}$$

Table 19. Solubility parameters for tritium diffusion at salt/solid interfaces

Parameter	FLiBe	Alloy-N	Graphite
k_0 [mol/m^{3}Pa^a]	9.3e-7	9.53e-1	1.9e-2
B [1/K]	4.27e-3	-	-
ΔH [J/mol]	-	1.07e4	-1.92e4
a = 1 or 0.5 for salt and solid respectively			

4.7 REACTOR KINETICS, FISSION PRODUCT, AND TRITIUM PROPERTIES

Reactor kinetics sets the power level of the reactor and thereby the fission product levels. Important characteristics for a salt-fueled system include permitting fission products to be born, decay, and transported around the loop or wherever fuel salt goes. A modified point kinetics model was created to handle this unique feature of salt-fueled systems. The model includes spatial generation and movement of precursor groups (Figure 16), fission products, and other trace substances. Reactivity feedback due to neutron absorption is also included. For transport purposes, the various products are modeled as trace substances. Greenwood and Betzler's forthcoming publication (Greenwood and Betzler In Review) provides a more detailed description of the kinetics model used in this paper.

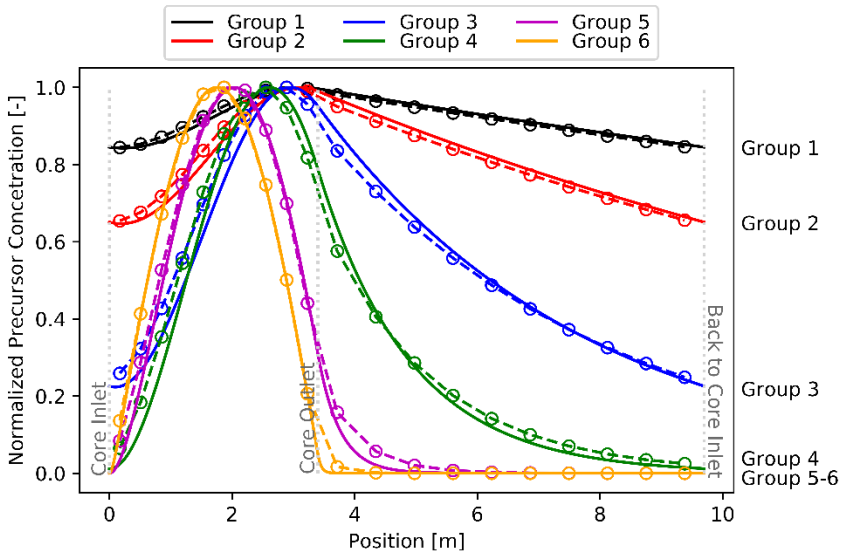

Figure 16. Comparison of analytic (dashed line) and numeric (solid line) models of the generation and movement of neutron precursors in a salt-fueled MSR (Greenwood and Betzler In Review).

The following subsections provide brief descriptions of the various parameters of the model. A nominal reactivity (ρ_0) associated with that of the fuel salt is required to operate the reactor at its nominal operating power. For this study, it was determined that $\rho_0 \cong 337\ pcm$. As with most specifics of this report, significant uncertainty remains in the parameters of salt reactors; the data provided are to illustrate the types of information that may be necessary for future studies and to inform future research needs. Given the uncertainty, the model was created so that modifications can be readily made for new or modified parameters. Furthermore, many of these parameters may change with time. The necessary logic for the values to change according to a user-specified time-dependent function is also included in the model.

4.7.1 Power Profile

The modified kinetics model used in this study is a point kinetics type model (Greenwood and Betzler In Review). The power profile is specified by the user instead of being determined by the physics of the system. All studies presented in this report used a uniform fission power distribution. This uniform distribution is also applied to the importance weighting on all reactivity feedbacks and fission product generation/consumption rates.

4.7.2 Temperature Reactivity Feedback

The temperature feedback in the core is driven by the fuel salt and the graphite (Table 20). In this report, it is assumed that the feedback from each contributed equally (i.e., no weighting factors) to the reactivity feedback of the fission power. The feedback parameters were taken from Robertson's ORNL-4541 (Robertson 1971).

Table 20. Core temperature feedback parameters

Parameter	Value	Unit
Type	Fuel salt, graphite	[-]
$T_{reference}$	649.114, 649.385	°C
α	-3.22e-5, 2.35e-5	K^{-1}

4.7.3 Neutron Precursor Groups

Six neutron precursor groups were chosen (Betzler et al. 2017a) (Table 21).

Table 21. Summary of neutron precursor group parameters

Parameter	Value	Unit
λ_i	0.0125,0.0318,0.109,0.317,1.35,8.64	s^{-1}
α_i	0.0320,0.1664,0.1613,0.4596,0.1335,0.0472	[-]
β	0.0065	[-]

4.7.4 Fission Source

The fission source, which drives the fission product composition was taken as an equal mixture of ^{235}U and ^{239}Pu in terms of contribution to fission (fissionSource) (Table 22). It was also assumed that their thermal and fast fissions contributed equally (fissionType) to the fission power. These values are used for demonstration purposes and will be different based on the reactor concept under consideration and will vary with time. These parameters impact the behavior of the power level and directly controls fission products generated.

Table 22. Summary of fission source parameters

Parameter	Value	Unit
Fuel type	^{235}U, ^{239}Pu	[-]
fissionSource	0.5,0.5	[-]
fissionType	{0.5,0.5}; {0.5,0.5}	[-]
$\bar{\nu}$	2.4	n/f
w_f	200	MeV
Σ_f	26	m^{-1}
Λ	1e-5	s

4.7.5 Fission Product Groups

Instead of tracking the full isotopic vector of over 2,200 nuclides, a smaller representative set of fission product groups is generated to demonstrate tracking of important elements throughout the fuel loop and to calculate space- and time-dependent decay heat. A full depletion model similar to that in the point depletion tool ORIGEN (Gauld et al. 2011) is computationally intractable due to the very large number of isotopes and necessary optimized solvers to generate solutions of such a large matrix problem. While integrating ORIGEN with the dynamic simulation functionality is an option, it is outside the scope of this work, which focuses on tracking isotopes within the fuel loop and processing systems.

The reduced set of isotopes is generated using ENDF-VII.1 data for independent fission yields, decay constants, and decay Q values for ^{235}U and ^{239}Pu (Chadwick et al. 2011). Hundreds of fission products for each isotope contribute collectively to decay heat; there is no reduced set of isotopes that is representative of both the energy and time release of decay heat energy. If all isotopes are tracked, the decay heat is calculated easily from the decay rate of radioisotopes and the decay Q values, which is the total energy released in beta, gamma, and other radiation. An empirical model for decay heat is not implemented because it is less physical and does not consider the individual isotopes that contribute to decay heat. It is desirable to track elemental groups moving through the system; these are obtained from collapsing isotopic and elemental information appropriately.

These objectives result in two categorizations that are merged into one single set of fission product groups. The first categorization is among elemental groups: gases, noble metals, fluorides, seminoble metals, rare earth elements, and discard (Table 23) (Betzler et al. 2017b). The second categorization is among half-lives, where the hundreds of fission products are divided into seven categories from the shortest- to longest-lived isotopes (Table 24). Thus, there are 24 fission product groups in this simplified model. Group decay constants and Q values are calculated by weighting the data by the independent yield of the constituent fission products. The sum of the constituent yields becomes the yield of a given group. For simplicity, the shortest-lived fission product group will decay into the next shortest fission product group with the same constituent elements. While this is not physically true in all cases, this is intended to serve as a simple model for demonstration purposes. Due to their importance in reactivity feedback and source term characterization, four isotopes are not grouped with the others: ^{135m}Xe, ^{135}Xe, ^{136}I, and ^{3}H. An alternative set of isotopes is generated for grouping the seminoble metals, fluorides, rare earth elements, and discard categories into a single group.

This work does not represent a conclusion on how fission products should be grouped. Rather, it is an initialization point for discussion on ways to capture the important physics associated with fission products in a smaller, tractable set appropriate for system level models.

Table 23. Fission product elemental groups

Group	Seminoble metals	Noble Metals	Gases	Fluorides	Rare earth elements	Discard
No. of fission products	281	269	51	51	251	95

Table 24. Fission product half-life groups

Half-life upper bound [s]	0.1	1.0	20.0	1200.0	2.0E5	-	Stable
No. Of fission products	70	180	178	172	106	100	187

4.7.6 Tritium

The principle source of tritium in a system using FLiBe as the carrier salt is from neutron interaction with the FLiBe (Stempien 2015). The major production pathways of tritium in a FliBe-based system are shown below. The generation rate of tritium is a function of the fission power and the cross section for tritium generation (σ_{H3}). Based on this interaction and the absorption of neutrons, the composition of the carrier salt changes with time (i.e., change in ^{6}Li and ^{7}Li) from a specified initial state. This change over time is captured in the model. The initial state of the a LiF-BeF_2 (67–33 mol%.) carrier salt was 99.995% enriched in ^{7}Li. All tritium is generated in the single core model. It is assumed that no tritium is generated in the reflector region.

$$^{6}_{3}Li + ^{1}_{0}n \rightarrow ^{4}_{2}He + ^{3}_{1}H$$

$$^{7}_{3}Li + ^{1}_{0}n \rightarrow ^{4}_{2}He + ^{1}_{0}n + ^{3}_{1}H$$

$$^{9}_{4}Be + ^{1}_{0}n \rightarrow ^{6}_{2}He + ^{4}_{2}He$$

$$^{6}_{2}He \rightarrow ^{6}_{3}Li + e^{+} \left(t_{\frac{1}{2}} = 0.8sec\right)$$

Table 25. Summary of tritium parameters

Substance	^{6}Li, ^{7}Li, ^{9}Be, ^{6}He	[-]
λ	0, 0, 0, log(2)/0.8	s^{-1}
σ_a	148.032, 0, 3.63e-3, 0	m^2
σ_{H3}	148.026, 1e-3, 0, 0	m^2

5. RESULTS

A few scenarios were simulated to enhance understanding of the steady-state and transient behavior of the model and to demonstrate the type of information available to the user. Note that in an MSR there is no true steady-state, so within the context of this report, *steady-state* refers to a condition in which fast evolving transients have died out, leaving only slowly changing effects such as the results of very long-lived fission products. Table 26 presents brief descriptions of each of the case scenarios. The following sections provide results from each of the cases simulated and descriptions of the observed behaviors. All simulations were performed using the commercial integrated development environment for Modelica called Dymola 2018FD01 (Dassault Systemes n.d.).

Table 26. Case descriptions

Case	Description
1. Steady-state	Steady-state simulation at nominal parameters
2. Transient – pump trip	Pump coast down to 0.1% of nominal flow rate

5.1 CASE 1 – STEADY-STATE BEHAVIOR

This section presents a select set of parameters of the model operating at a steady-state condition. Simulation statistics of the steady-state simulation are provided in Table 27. All subsequent tests begin from the result of this simulation. A very small selection of available steady-state variables is presented in Table 28 – Table 31.

Table 27. Steady-state simulation summary

Parameter	Description
Simulation time	172,800 seconds (2 days)
CPU time	509 seconds
Sampling frequency	1 Hz
Solver	Esdirk-45a

Table 28. Steady-state inlet and outlet temperature of principle components (°C)

	Inlet	Outlet
Reactor	837.8	947.7
Core	837.8	956.1
Reflector	837.8	837.9
PHX PFL side (tube)	935.9	837.4
PHX PCL side (shell)	766.2	865.6
SHX PCL side (shell)	856.4	756.1
SHX BOP side (tube)	707.5	813.7
Drain tank	947.7	724.2

Table 29. Steady-state average core and reflector temperatures (°C)

		Average	Max	Min
Core	Salt	902.5	956.1	849.5
	Graphite	902.8	956.1	849.6
Reflector	Salt	837.9	837.9	837.8

Graphite	837.9	838.0	837.8

Table 30. Steady-state pressures in PFL

Variable	Value	Unit
Core Inlet Pressure	0.22	MPa
Core Outlet Pressure	0.19	MPa
Pump Bowl Pressure	0.12	MPa
Pump Discharge Pressure	1.4	MPa

Table 31. Steady-state flow rates

Variable	Value	Unit
PFL $\dot{m}$	5544	kg/s
PCL $\dot{m}$	2797	kg/s
PFL τ	25.08	s
PCL τ	31.37	s

Table 32. Steady-state power in the core (decay heat does not include loop contribution)

Total	735	MW
Fission	724	MW
Decay-heat	11	MW

Table 33. Steady-state heat rejection from decay heat removal system

DrainTank	11	MW
Charcoal bed	394	kW

Table 34. Tritium generation and release rate

^{3}H generation	4E+16	atoms/s
^{3}H release	7E+07	atoms/s

Figure 17 presents the temperature profile throughout the PFL. The uniform power distribution yields a linear increase in temperature. At the core outlet, the temperature drops due to the mixing of the small

amount of cold salt which passed through the reflector region. The hot salt then passes through the PFL heat exchangers and returns to the core.

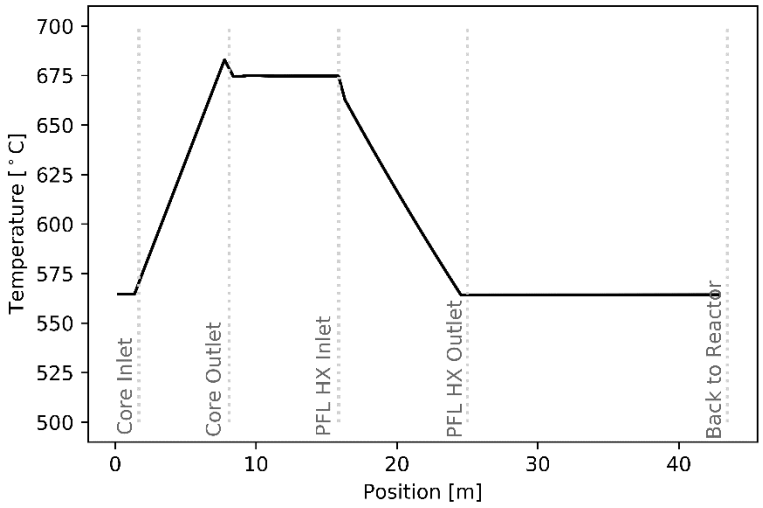

Figure 17. Steady-state temperature distribution as a function of position in the PFL.

Figure 18 presents the distribution of a select number of fission products as a function of position in the PFL. Although limited to only three substances, the plot demonstrates several important features. The tritium in the loop decreases between the inlet of the reactor to the inlet of the core and once again from the outlet of the core to the outlet of the reactor. This decrease is due to diffusion of tritium into the graphite of the axial reflectors, which have a significant amount of surface area for transfer. The tritium builds up as the fuel salt passes through the core as a function of the power profile. The tritium decays slowly ($t_{1/2}$ = 12.3 years), so impact from decay as it moves around the core is not noticeable in the figure. As the salt passes through the PFL heat exchangers, tritium passes through the tube walls to the PCL and ultimately to the environment. The precursor presented is Group 5, which has a relatively short half-life. The precursor builds up in the core and then quickly decays as the salt moves through the core. Depending on the half-life of the precursor and the salt flow rate, the return concentration to the core will vary from zero to some larger, significant value. ^{135}Xe builds up in the core and decays very little as it moves around the loop ($t_{1/2}$ = 9.2 hours). However, the off-gas system is connected to the PFL at approximately 10 m. The decrease in xenon concentration due to the long hold-up period in the charcoal adsorber bed in the off-gas system can be readily observed.

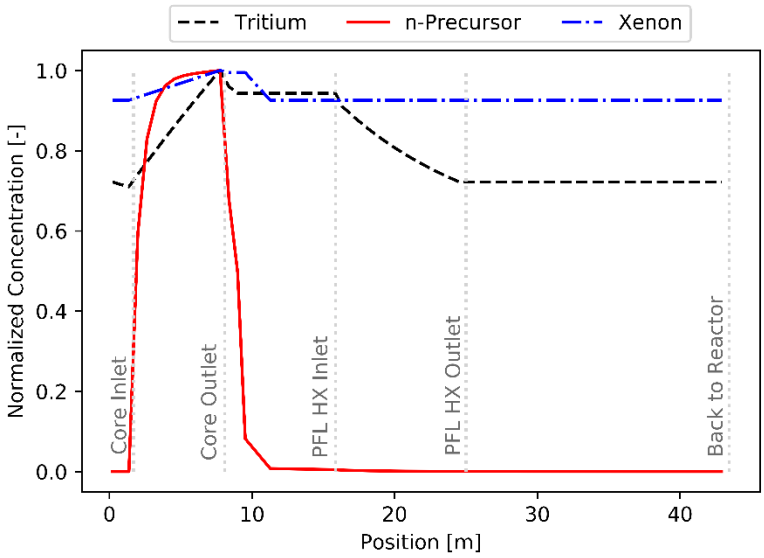

Figure 18. Steady-state normalized concentrations distribution of select precursors as a function of position in the PFL.

5.2 CASE 2 – BEHAVIOR UNDER PFL PUMP TRIP SCENARIOS

The initial transient cases performed simulated various combinations of PFL pump with and without control rod action.

Scenario	λ (s^{-1})	ρ_{CR} (pcm)
A	1/40	0
B	1/20	0
C	1/40	-300
D	1/40	-3,000

provides a brief description of each of the scenarios and scenario labels for reference. As appropriate, per the scenario description, the pump flow rate was exponentially decreased with a decay constant (λ) at time = 172,800 seconds and an offset of 0.1% of the nominal steady-state flow rate. The small amount of flow rate was permitted to avoid any potential numerical issues associated with zero flow. For cases with control rod action, negative reactivity of different amounts (ρ_{CR}) was inserted at a constant rate of ~1.5 inches per second (i.e., 150 seconds to fully insert an 18 ft. control rod).

Table 35. Case 2 – Scenario description

Scenario	λ (s^{-1})	ρ_{CR} (pcm)
A	1/40	0
B	1/20	0
C	1/40	-300
D	1/40	-3,000

The overall temperature feedback of the modeled MSR is negative, so as the mass flow rate decreases (Figure 19), it causes the reactor fission power to decrease proportionally over time (Figure 20) as the kinetics of the reactor strive to correct the imbalance from the reference temperature state. Less flow increases the temperature of the reactor, which adds negative reactivity feedback to the power kinetics (Figure 21). The hump in decay heat within the core is likely attributable to short-lived decay products that were decaying in other portions of the PFL, but now they are decaying in the core due the decreased

flow of salt. Depending on the amount reactivity and its insertion rate, the final temperature of the core may increase or decrease from the nominal value (Figure 22).

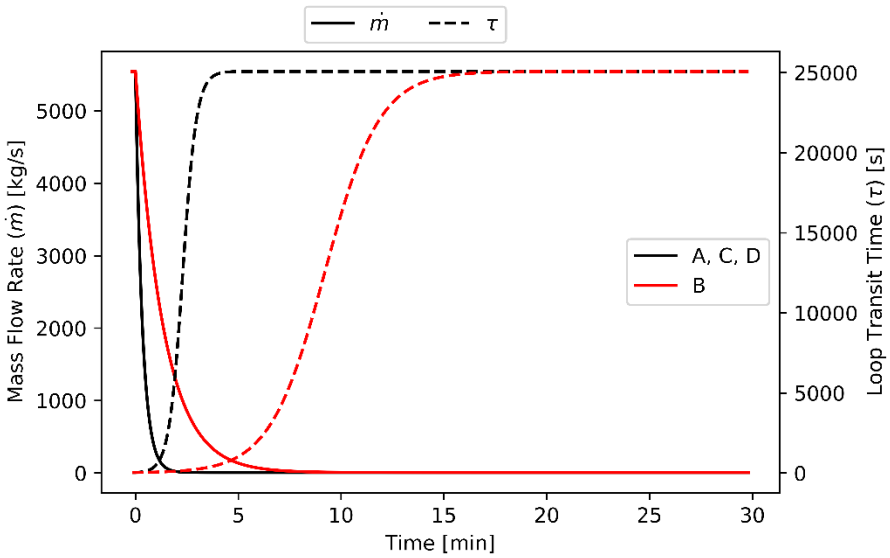

Figure 19. Case 2 – Mass flow rate and loop transit time as a function of time.

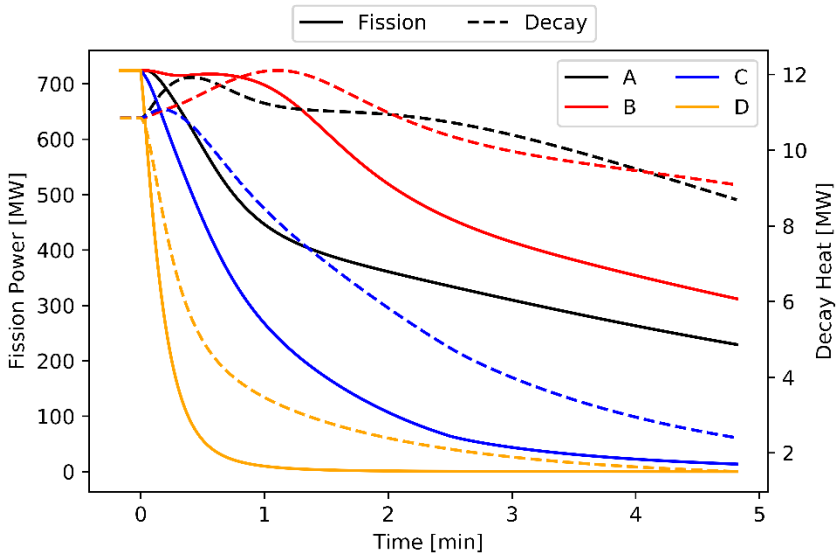

Figure 20. Case 2 – Fission and decay heat as a function of time.

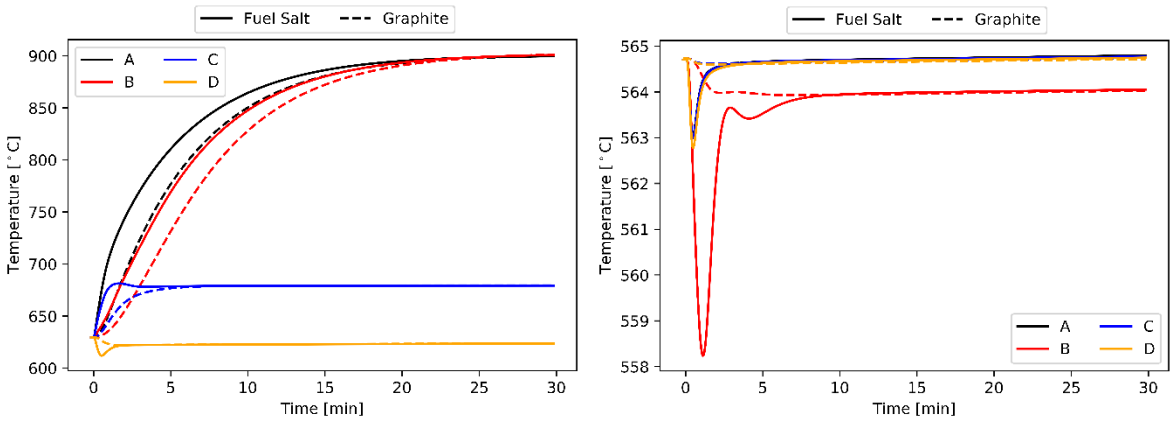

Figure 21. Case 2 – Average temperature of fuel salt and graphite as a function of time for the core (left) and radial reflector (right).

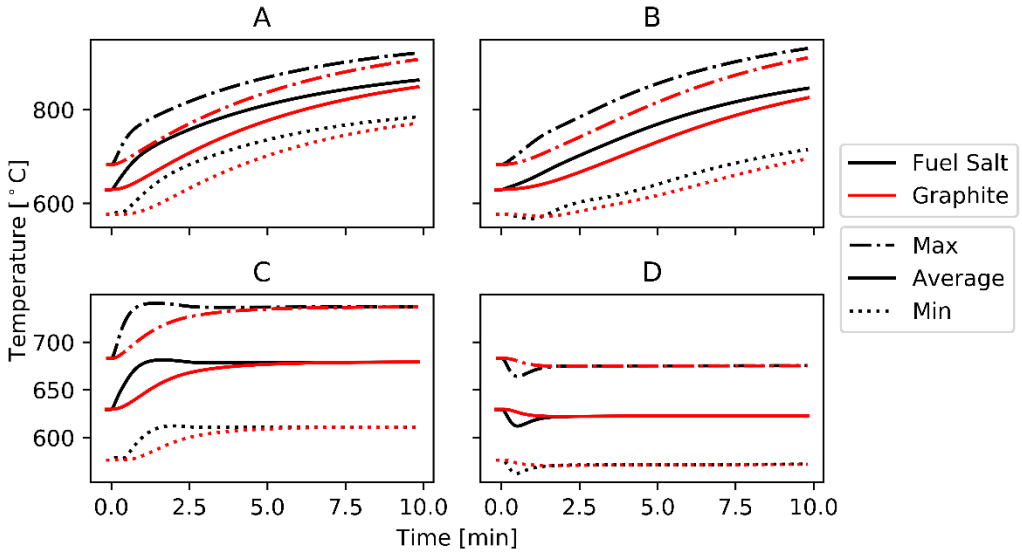

Figure 22. Case 2 – Maximum, average, and minimum fuel and graphite temperature in the core for each case scenario.

The pressure behavior of the reactor is principally driven by the flow rate in the loop (Figure 23). Once the flow reaches its new setpoint, but the reactor has not yet reached thermal equilibrium. Over a longer period, slight pressure changes occur to the shift in salt density with temperature. Figure 24 and Figure 25 show the behavior of the primary heat exchanger (PHX) and secondary heat exchanger (SHX) over time. Initial changes in temperature of the PHX are dominated by the change in temperature of the PFL, causing a peak in the tube inlet. As time progresses, the small flow rate of salt through the heat exchangers, with the primary circulation loop (PCL) continuing to operate at nominal flow rate, approaches a very small ΔT across the heat exchanger in accordance with the power of the reactor. Similar behavior is seen in the SHX as the balance of plant (BOP) flow is also held at nominal flow rate.

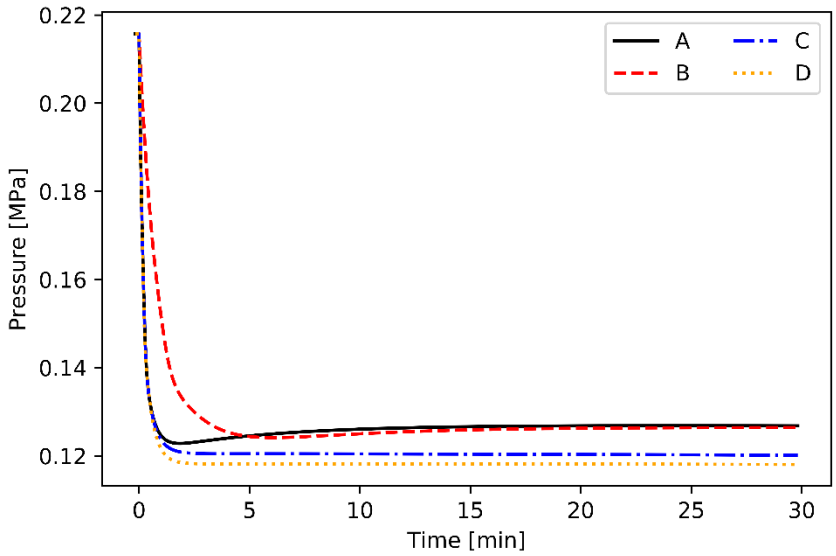

Figure 23. Case 2 – Core inlet pressure as a function of time.

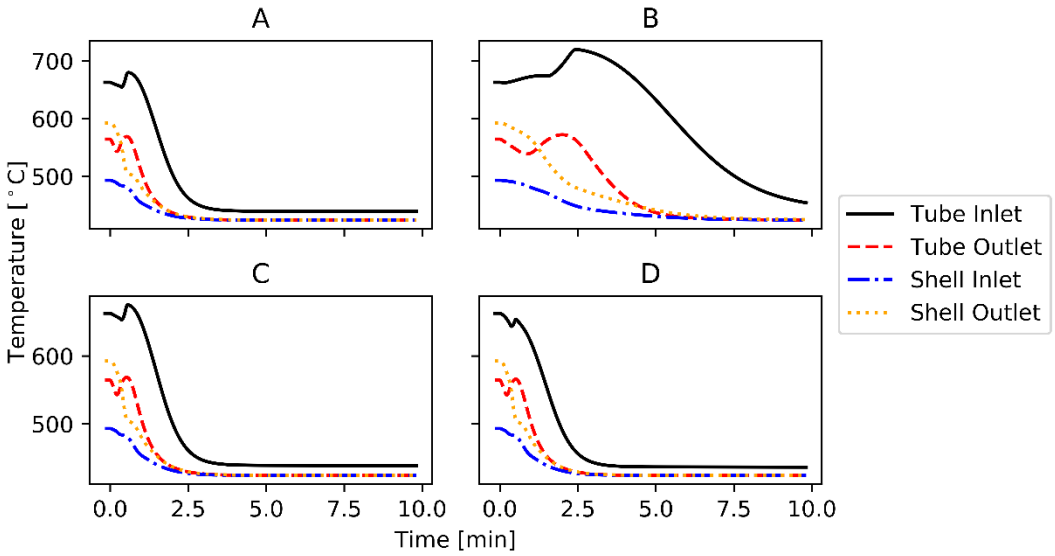

Figure 24. Case 2 – PHX inlet and outlet temperature as a function of time (Tube = PFL; Shell = PCL).

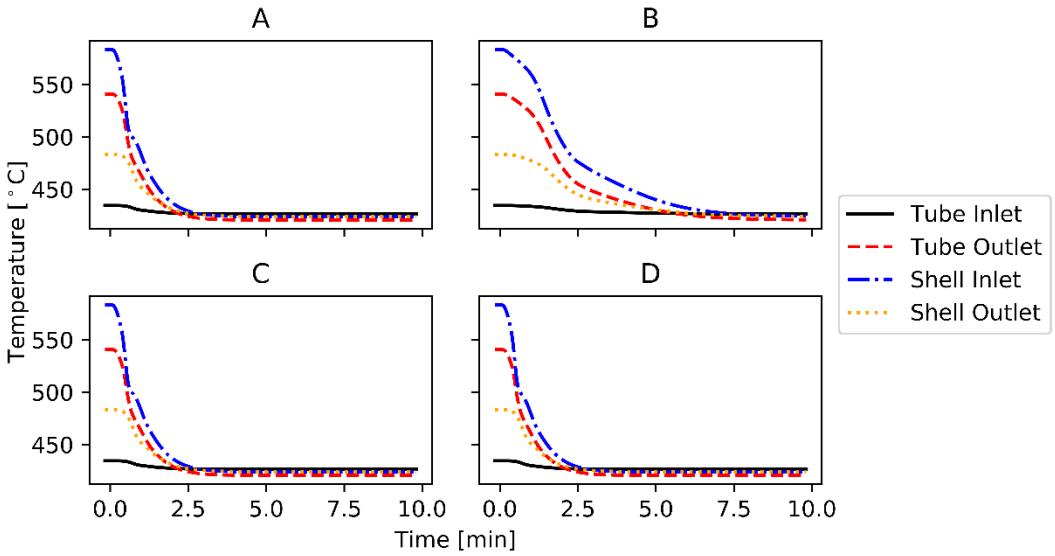

Figure 25. Case 2 – SHX inlet and outlet temperature as a function of time (Tube = BOP; Shell = PCL).

Figure 26 demonstrates the relative or normalized rate of tritium release from the system. As expected, the generation rate of tritium tracks the fission power. The flow rate of the PFL sets the concentration gradient and diffusion coefficient at the PHX of tritium and therefore sets the rate of transfer between the PFL and PCL (to PCL). Therefore, tritium transfer decreases in accordance with the PFL flow rate. However, the release to the environment changes little directly due to flow rate changes in the PFL. Instead, concentration gradient changes and solubility changes due to shift in temperatures drive the small bump in each scenario's release of tritium to the environment.

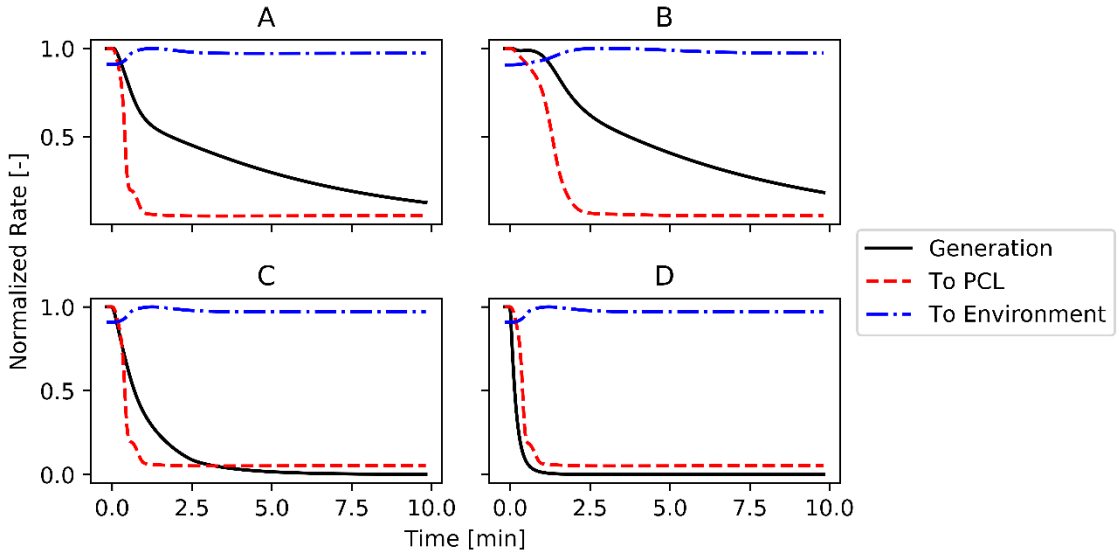

Figure 26. Case 2 – Normalized tritium generation and release rate as a function of time.

Figure 27 through Figure 30 provide surface plots of each of the scenarios as a function of time and position in the loop. These plots enhance understanding of the overall behavior of the loop over a transient event. The changes in temperatures, concentrations, etc., discussed above hold true and can be

examined spatially to clarify the scenario over time. Figure 27 provides the temperature behavior of the reactor over time, showing the rise in core temperature, for example. Figure 28, Figure 29, and Figure 30 illustrate the change in tritium, neutron precursor group 5, and ^{135}Xe concentration on a salt mass basis. The neutron precursor group 5 is a short-lived precursor. Therefore, the plot demonstrates that these types of transients have little impact on group 5's behavior as it decays away so quickly. When the reactor shuts down, regardless of the scenario, the Xe concentration builds up over time due the decay of iodine. In the figure, the Xe concentration has just barely reached a maximum and is starting to diminish due to iodine having decayed to low levels and Xe decay becoming the dominating factor in the Xe balance.

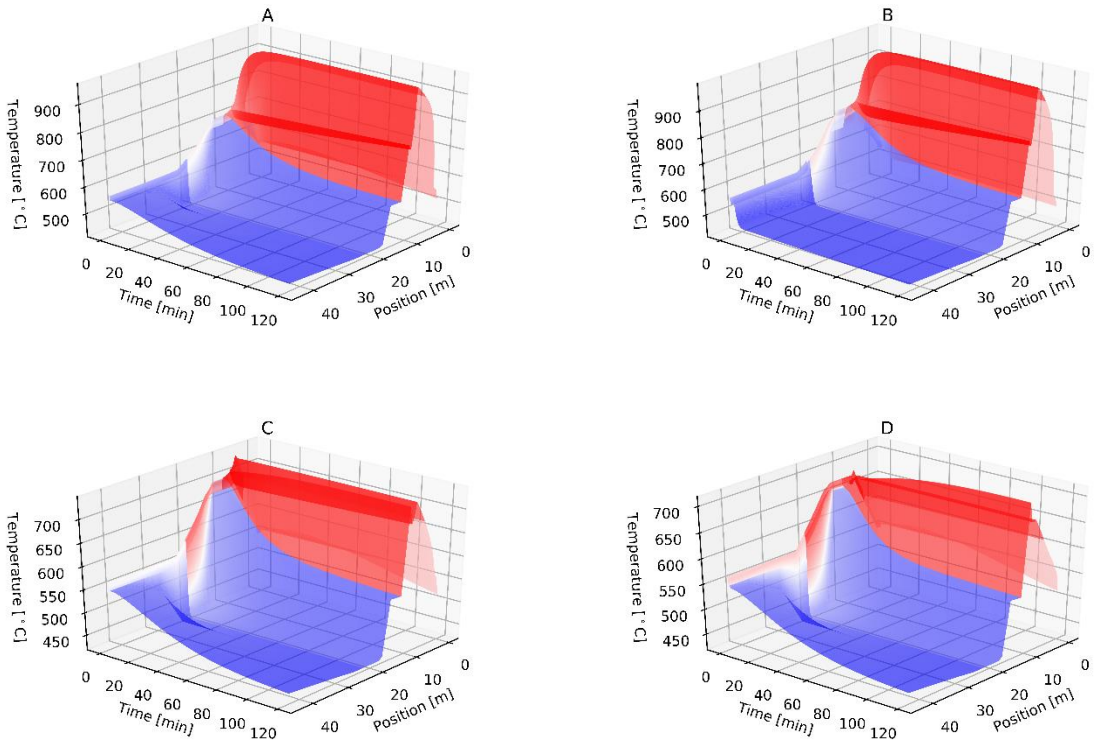

Figure 27. Case 2 – Temperature for each scenario as a function of time and position.

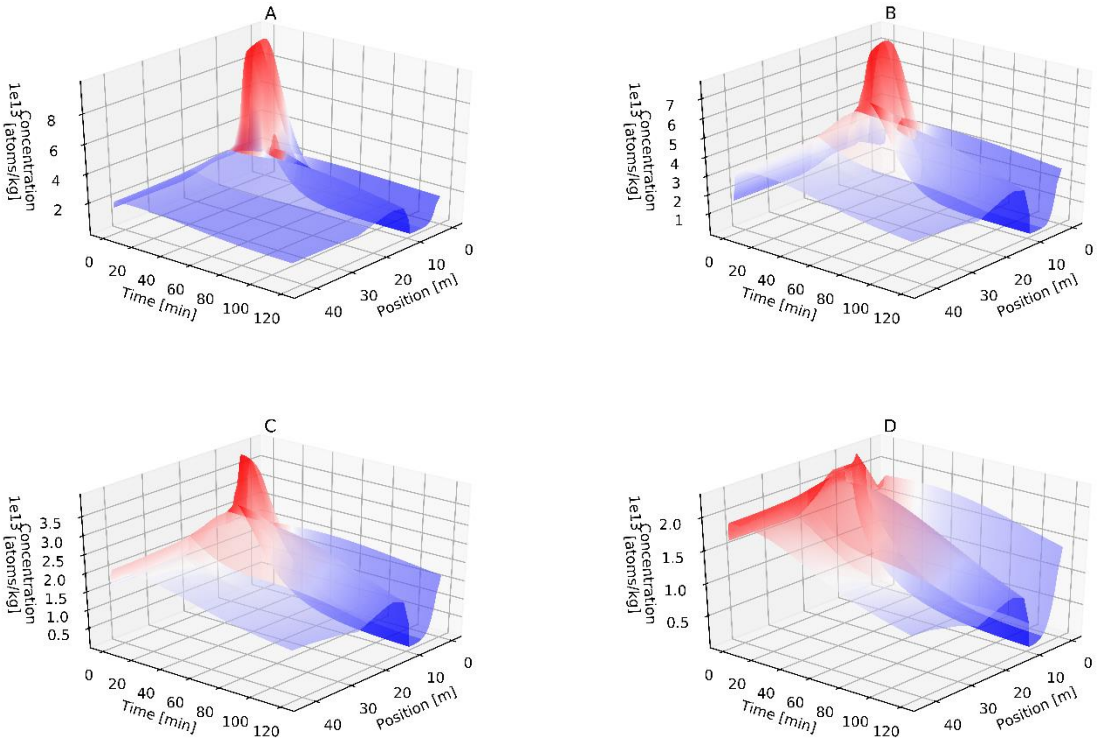

Figure 28. Case 2 – Tritium concentration for each scenario as a function of time and position.

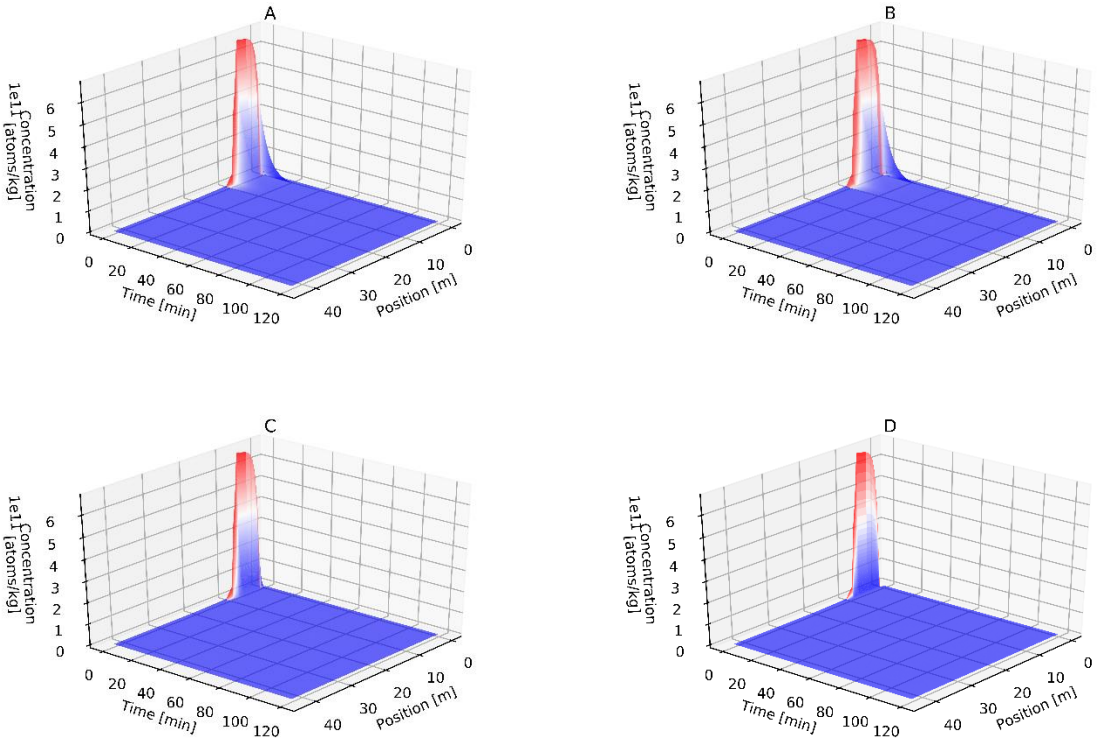

Figure 29. Case 2 – Neutron precursor group 5 concentration for each scenario as a function of time and position.

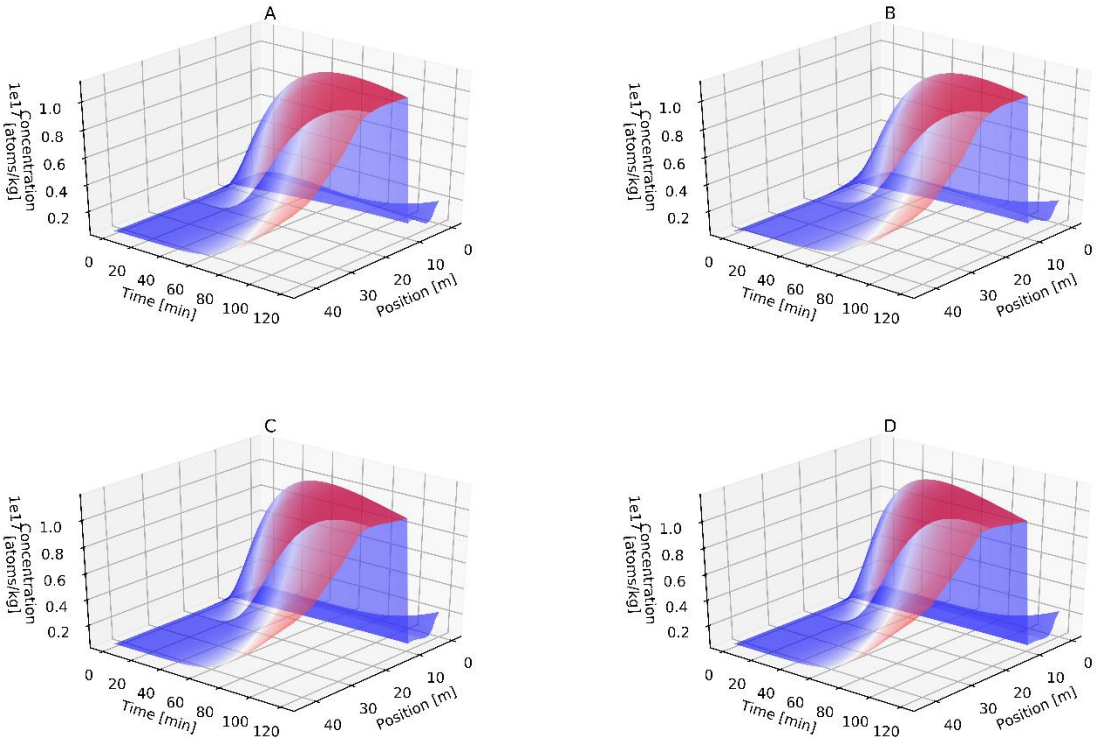

Figure 30. Case 2 – ^{135}Xe concentration for each scenario as a function of time and position.

5.3 CASE 3 – SIMULATION IN CHANGE OF FISSILE MATERIAL

Over the operating life of an MSR, the parameters which drive the power kinetics of the reactor will change with time. For example, as fissile material is consumed, the fissile material contribution to fission power will likewise change. This change will impact the kinetics of the reactor through such parameters as β, the effective delayed neutron fraction. These time-dependent changes will impact and modify the behavior of the reactor. However, since the fissile fuel resides in the liquified salt, there are options to alter the fuel composition online. These actions would likely be performed at staged short-term intervals. One alternative scenario in which the salt is modified is in the case that bad actors attempt to divert fissile material. This case presents a simple scenario in which β is decreased by a fraction of the initial value ($\beta_0 = 0.0065$) over a period of 60 minutes (Table 36). All other parameters are unchanged.

Table 36. Case 3 – Scenario description

Scenario	Δβ (-)
A	-0.001*β_0
B	-0.01*β_0

As negative variation of β the reactivity feedback (ρ) versus β becomes more positive in the kinetics power equation, this increases the reactor fission power in accordance with the change in β (Figure 31). The increased fission power then increases the fission product concentrations and thereby the decay heat. As the power increases, the temperature of the reactor also increases, although the increase is not directly proportional, as the higher fuel salt temperature increases the driving temperature gradient at the PHXs

(Figure 32). The increases in fuel salt temperature also slightly impact the pressure due to changes in fuel salt density (Figure 33).

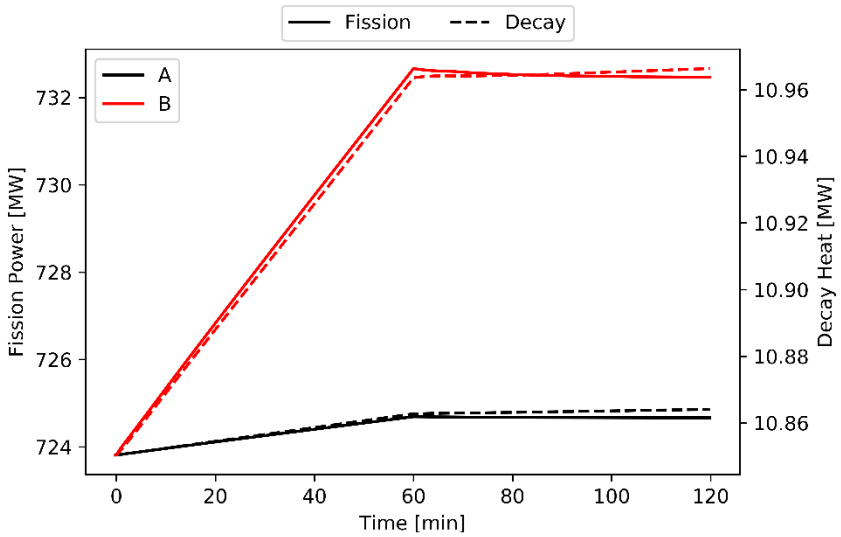

Figure 31. Case 3 – Fission and decay heat as a function of time.

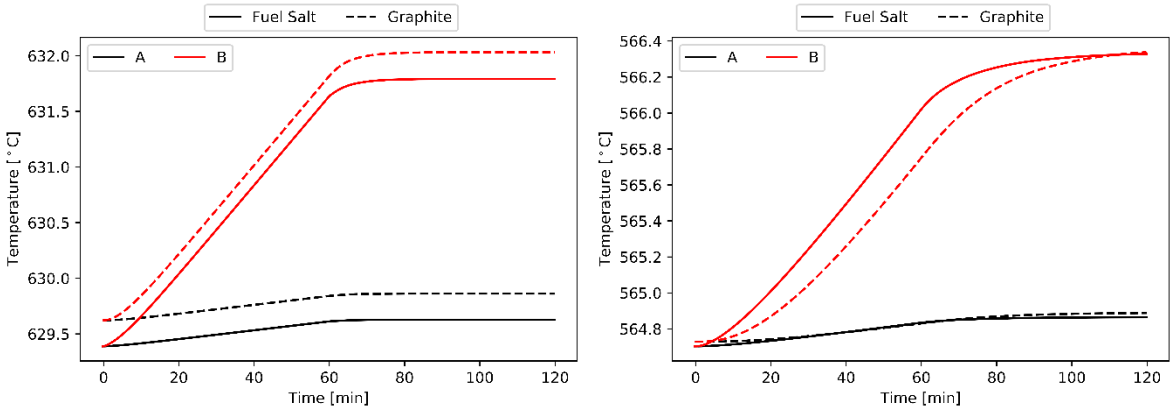

Figure 32. Case 3 – Average temperature of fuel salt and graphite as a function of time for the core (left) and radial reflector (right).

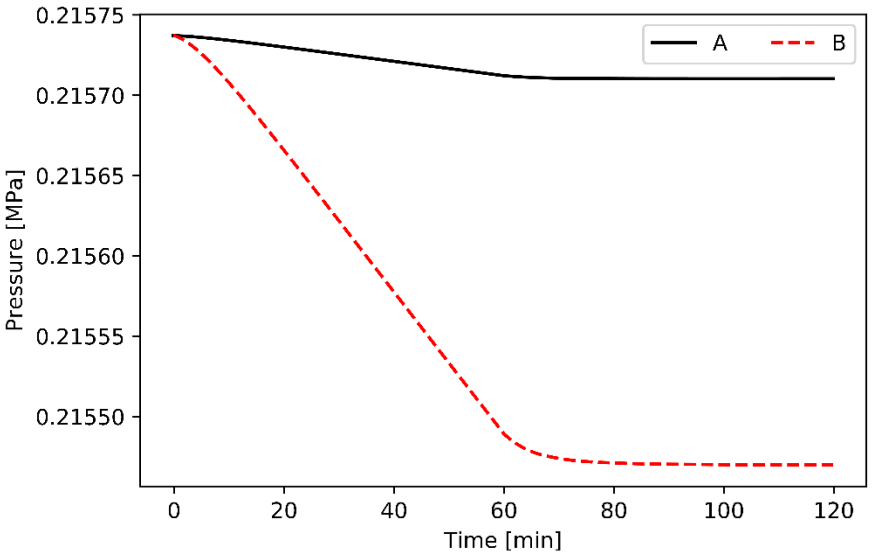

Figure 33. Case 3 – Core inlet pressure as a function of time.

6. CONTINUING AND FUTURE WORK

This report demonstrates the feasibility of incorporating a large variety of physics and capabilities into a single model to investigate MSRs. Many improvements and extensions of this work are possible to improve the type of steady-state and transient scenarios that can be analyzed, types of reactors and processes that can be incorporated, and overall usability of the tool for users (as opposed to developers). The list of various improvements and scenarios to be investigated is not stagnant, as growing understanding of MSR behavior, through this and other work, will drive all continuing and future work. However, several items have been identified as possible work that would progress the overall ability to understand MSRs.

TRANSFORM System Modeling Tool

The following list a non-exhaustive list of activities directly related to modeling that are likely areas of future work for the TRANSFORM system modeling tool.

- Create dedicated MSR components to simplify the use of the tool for MSR applications and to reduce user error
- Improve restart capabilities to enable mid/end-cycle transient simulations
- Perform sensitivity analysis of physics parameters to rank parameter significance
    - This is important for focusing future work and can be scenario-dependent
    - Examples include kinetics, heat transfer, and mass transfer parameters
- Incorporate balance of plant models to understand coupled behavior
- Increase representative channels in core model
- Improve/identify fission product groups for scenarios of interest
    - Includes the investigation of methods to extend the number of fission products that can be incorporated to reduce uncertainty/assumptions
- Couple model with ORIGEN for improved workflow options
- Add transient fissile material behavior (e.g., transmutation, burnup)
- Add component-dependent thermos-physical media properties
- Introduce level tracking pipe models to investigate fill/drain scenarios
- Introduce additional processes of interest
    - Examples include tritium capture, redox control, separations processes, etc.
- Add chemistry models to capture processes such as corrosion, T_2/TF ratios, and redox potential
- Introduce a multigroup 1D and 2D neutron diffusion model in the core to better capture dynamic behavior associated with a fluid-fueled system
- Add radiative heat transfer option to models
- Compare results to other codes (e.g., SCALE) for model validation and identification of areas of improvement
- Continue to improve QA procedures and documentation
- Demonstrate high-low model fidelity coupling (e.g., VERA-MSR and TRANSFORM).

An additional activity associated with TRANSFROM and Modelica is a review of industrial applications of Modelica. This activity would attempt to identify examples of Modelica use in such areas as licensing, design, and safety applications (e.g., automotive and aerospace). Limitations of the Modelica languages use in such applications as licensing and safety, if any, would be identified. This activity will help shape long term end-use applications and model development activities.

Additional Activities

Other activities that are separate from modeling activities yet are related include experiments critical to understanding the behavior of MSRs for licensing, safeguards, and security investigations. The following is a non-exhaustive list of identified activities:

- Identify credible accident scenarios
- Identify principal reactions/processes in critical physical phenomena
    - Examples include fission product gas behavior near and above the solubility limit, rate-determining steps in corrosion processes (e.g., Cr depletion from heat exchangers) including solubility information at interfaces (e.g., liquid/solid), and diffusion coefficients of species in molten salts and solid materials (e.g., graphite and various steels)
    - For dynamic (e.g., accident) scenarios, reaction rates, solubility laws, etc., must be defined for identified phenomena. If not available, experiments must be designed and performed to determine those parameters necessary for transient modeling, such as the model in this report
    - This activity should be coupled with sensitivity analysis to focus efforts on reducing the uncertainty of the principal parameters driving the identified physical phenomena.

6.1 APPLICATION TO OTHER MSR TYPES

This report presents demonstrations of the types of information necessary to perform dynamic system model evaluations of MSRs. Depending on the design (i.e., fast vs thermal, online-refueling vs complete separations) more or less information may be necessary. However, various models and capabilities were implemented in such a way as to remain as generic as possible. Therefore, the tool developed from this work can be readily adapted and expanded for the design required and will likely be applied to specific designs in the future such as salt-fueled fast chloride reactors and pebble-bed type salt-cooled reactors.

When applying the tool to other reactor types, there can be a variety of differences and similarities. In general, new models can be readily created and integrated into any design. Therefore, the user is not limited to the components available in the library. They are free to develop their own components or import them from other compatible Modelica libraries or perform combinations thereof using tools with functional mock-up interface (n.d., FMI) support (e.g., ANSYS, Matlab, etc. See http://fmi-standard.org/tools/ for a full list of tools). Within the TRANSFORM library itself, users have direct access to the all the source code and can duplicate and modify existing components to suit their needs.

For example, if the user chooses to specific an alternative salt than FLiBe, which was used in this effort, the user can select alternative media or create his or her own using existing templates. Similar analogies hold true for physical phenomena such as heat and mass transfer correlations (Figure 34). If components with similar parameters exist, then the user can exchange components while retaining all common information shared between the models, as shown in Figure 35. For example, it is questionable to model the core of a fast reactor with point kinetics or even with 1D kinetics. However, without a detailed design, much of the remaining facility may be like the MSDR generic concept for preliminary investigations. The user simply must define an appropriate kinetics model and fluid channel for the core and then exchange that with the existing one. Likewise, for a pebble bed reactor, a model of the pebble fuel can be created, used to replace the existing design, and aspects associated with fission product transport can be removed if not applicable. In this manner, a large variety of models tailored to the user's needs can be generated without a significant amount of time or effort.

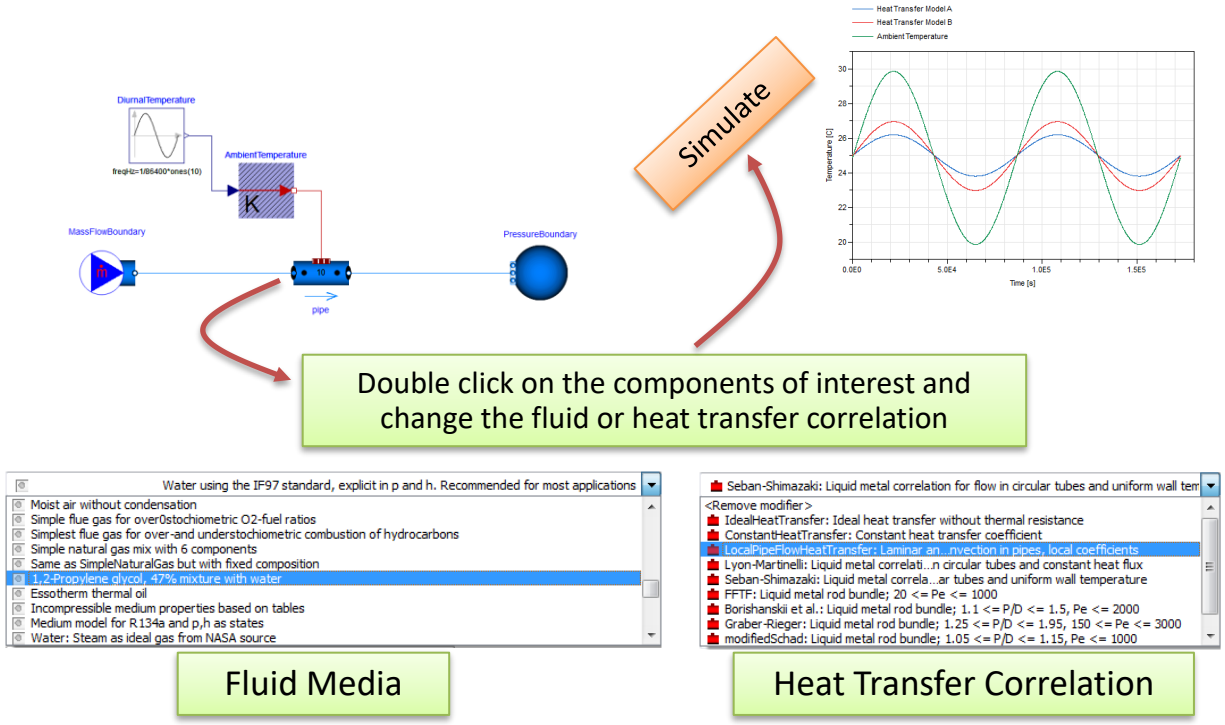

Figure 34. Example of one method to modify the fluid and heat transfer correlation used in components.

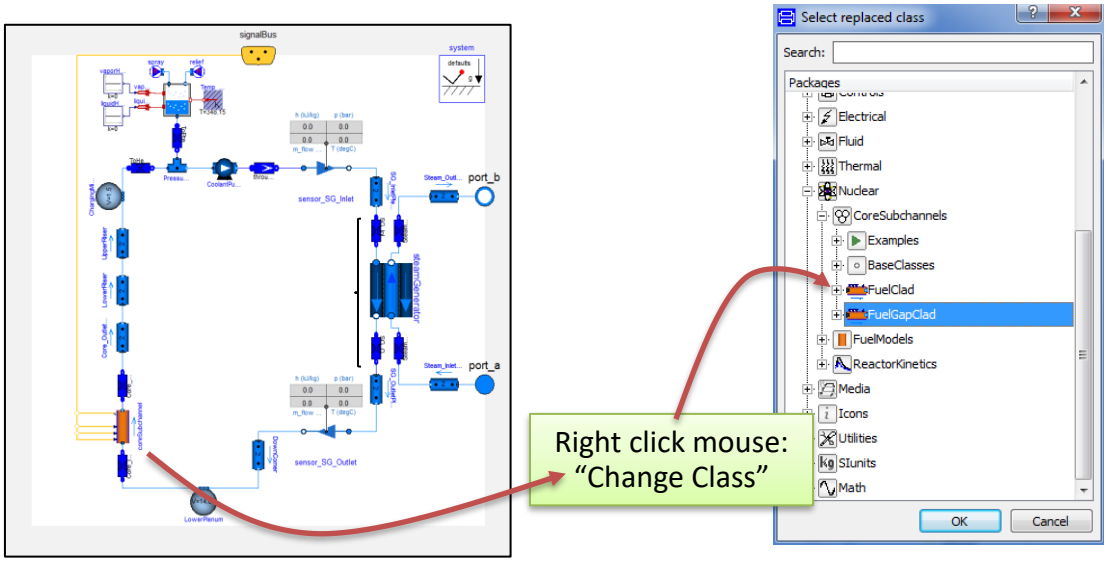

Figure 35. Example of a method to replace an existing component with a different component.

6.2 PARAMETRIC AND SENSITIVITY STUDIES

Using the Modelica language as a basis for modeling complex physical processes not only provides the ability to import or export models to tools which support FMI as mentioned previously, but Modelica simulations can read external files (i.e., C and Fortran) during simulation and can been run from popular languages adopted by the scientific community such as Python. There is a variety of tools, commercial and open-source, which permit parametric studies and optimization analysis of Modelica based systems

such as Optimica and RAVEN (Rabiti [2017] 2018). The RAVEN tool has been used to investigate the economic optimization of hybrid energy systems using models developed with TRANSFORM (Rabiti et al. 2017). Although the technology to perform true parallelization of Modelica-based models is an area of active research (Ozmen, Nutaro, and New 2016; Sjölund, Gebremedhin, and Fritzson 2013; Goteman and Roxling 2015; Gebremedhin and Fritzson 2014), Modelica models are routinely run in parallel on server clusters (e.g., sensitivity analysis).

7. SUMMARY

Fluid-fueled nuclear reactors, particularly molten salt reactors (MSRs), have recently gained significant interest. As with all reactors, modeling and simulation are key factors for advanced reactor design and licensing and will be required for the deployment of MSRs. This report outlines the development and implementation of a system-level model of a generic thermal salt-fueled MSR for steady-state and transient scenario investigations. The model is implemented in the ORNL TRANSFORM tool, a Modelica-based library for modeling thermal-hydraulic and other multi-physics systems. The design requirements of the model gave special consideration of the needs for licensing, safeguards, and security. As such, the model tracks the movement of fission products such as neutron precursor groups, xenon, and tritium throughout the primary fuel loop, off-gas and decay heat removal systems, and even diffusion of species, such as tritium, from the primary fuel loop to the environment. Additionally, the model presented represents an effort to identify needs and gaps that are needed to investigate dynamic behaviors of MSRs. The modeling concepts used in this study will be applied to additional studies of alternative reactor types and sensitivity studies to further the understanding of MSR behavior and assist in driving the goal of licensing MSRs.

8. REFERENCES

Bettis, E.S., Alexander, L.G., Watts, H.L.: Design Studies of a Molten-Salt Reactor Demonstration Plant. (1972)

Betzler, B.R., Powers, J.J., Brown, N.R., Rearden, B.T.: Implementation of Molten Salt Reactor Tools in SCALE. Presented at the International Conference on Mathematics & Computational Methods Applied to Nuclear Science & Engineering , Jeju, Korea January 16 (2017)(a)

Betzler, B.R., Powers, J.J., Worrall, A.: Molten salt reactor neutronics and fuel cycle modeling and simulation with SCALE. Ann. Nucl. Energy. 101, 489–503 (2017)(b). doi:10.1016/j.anucene.2016.11.040

Brown, N.R., Betzler, B.R., Carbajo, J.J., Wysocki, A.J., Greenwood, M.S., Gentry, C., Qualls, A.L.: Preconceptual design of a fluoride high temperature salt-cooled engineering demonstration reactor: Core design and safety analysis. Ann. Nucl. Energy. 103, 49–59 (2017). doi:10.1016/j.anucene.2017.01.003

Bulmer, J.J., Gift, E.H., Holl, R.J., Jacobs, A.M., Jaye, S., Koffman, E., McVean, R.L., Oehl, R.G., Rossi, R.A.: Fused Salt Fast Breeder Reactor Design and Feasibility Study. Oak Ridge National Lab. (ORNL), Oak Ridge, TN (United States) (1956)

Chadwick, M.B., Herman, M., Obložinský, P., Dunn, M.E., Danon, Y., Kahler, A.C., Smith, D.L., Pritychenko, B., Arbanas, G., Arcilla, R., Brewer, R., Brown, D.A., Capote, R., Carlson, A.D., Cho, Y.S., Derrien, H., Guber, K., Hale, G.M., Hoblit, S., Holloway, S., Johnson, T.D., Kawano, T., Kiedrowski, B.C., Kim, H., Kunieda, S., Larson, N.M., Leal, L., Lestone, J.P., Little, R.C., McCutchan, E.A., MacFarlane, R.E., MacInnes, M., Mattoon, C.M., McKnight, R.D., Mughabghab, S.F., Nobre, G.P.A., Palmiotti, G., Palumbo, A., Pigni, M.T., Pronyaev, V.G., Sayer, R.O., Sonzogni, A.A., Summers, N.C., Talou, P., Thompson, I.J., Trkov, A., Vogt, R.L., van der Marck, S.C., Wallner, A., White, M.C., Wiarda, D., Young, P.G.: ENDF/B-VII.1 Nuclear Data for Science and Technology: Cross Sections, Covariances, Fission Product Yields and Decay Data. Nucl. Data Sheets. 112, 2887–2996 (2011). doi:10.1016/j.nds.2011.11.002

Dassault Systemes: Dymola Systems Engineering, https://www.3ds.com/products-services/catia/products/dymola/

Fuderer, A.: Activated Carbon Adsorbent with Increased Heat Capacity and the Production Thereof, (1985)

Gauld, I.C., Radulescu, G., Ilas, G., Murphy, B.D., Williams, M.L., Wiarda, D.: Isotopic Depletion and Decay Methods and Analysis Capabilities in SCALE. Nucl. Technol. 174, 169–195 (2011). doi:10.13182/NT11-3

Gebremedhin, M., Fritzson, P.: Automatic task based analysis and parallelization in the context of equation based languages. Presented at the (2014)

Goteman, A., Roxling, V.: GPU Usage for Parallel Functions and Contacts in Modelica, http://lup.lub.lu.se/luur/download?func=downloadFile&recordOId=7869349&fileOId=7869358, (2015)

Greenwood, M.S.: TRANSFORM-Library: A Modelica based library for modeling thermal hydraulic energy systems and other multi-physics systems. (2017)

Greenwood, M.S., Betzler, B.R.: Modified Point Kinetic Model for Neutron Precursors and Fission Product Behavior for Fluid-Fueled Molten Salt Reactors. Nucl. Sci. Eng. (In Review)

Greenwood, M.S., Cetiner, M., Fugate, D., Hale, R., Harrison, T., Qualls, A.: TRANSFORM - TRANsient Simulation Framework of Reconfigurable Models, (2017)

Haubenreich, P.N., Engel, J.R.: Safety Calculations for MSRE. Oak Ridge National Laboratory, Oak Ridge, TN (United States) (1962)

IAEA: The Structure and Content of Agreements Between the Agency and States Required in Connection with the Treaty on the Non-Proliferation of Nuclear Weapons. International Atomic Energy Agency (1972)
Ingersoll, D.T.: Status of Physics and Safety Analyses for the Liquid-Salt-Cooled Very High-Temperature Reactor (LS-VHTR). Oak Ridge National Lab. (ORNL), Oak Ridge, TN (United States) (2005)
Ingersoll, D.T., Forsberg, C.W.: Status of Preconceptual Design of the Advanced High-Temperature Reactor (AHTR). Oak Ridge National Lab. (ORNL), Oak Ridge, TN (United States) (2004)
Ingersoll, D.T., Forsberg, C.W., MacDonald, P.E.: Trade Studies for the Liquid-Salt-Cooled Very High-Temperature Reactor: Fiscal Year 2006 Progress Report. Oak Ridge National Lab. (ORNL), Oak Ridge, TN (United States) (2007)
Kirillov, P.L.: Thermophysical Properties of Materials for Nuclear Engineering. Institute for Hat and Mass Transfer in Nuclear Power Plants (2006)
Mays, G.T., Smith, A.N., Engel, J.R.: Distribution and Behavior of Tritium in the Coolant-Salt Technology Facility. Oak Ridge National Lab. (ORNL), Oak Ridge, TN (United States) (1977)
Modelica Association: Modelica Standard Library. Modelica Association (2018)
NRC: Nuclear Power Plant Licensing Process Fact Sheet. Nuclear Regulatory Commission (2010)
Ozmen, O., Nutaro, J.J., New, J.R.: Parallel Execution of Functional Mock-up Units in Buildings Modeling. (2016)
Qualls, A.L., Betzler, B.R., Brown, N.R., Carbajo, J.J., Greenwood, M.S., Hale, R., Harrison, T.J., Powers, J.J., Robb, K.R., Terrell, J., Wysocki, A.J., Gehin, J.C., Worrall, A.: Preconceptual design of a fluoride high temperature salt-cooled engineering demonstration reactor: Motivation and overview. Ann. Nucl. Energy. 107, 144–155 (2017). doi:10.1016/j.anucene.2016.11.021
Qualls, A.L., Brown, N.R., Betzler, B.R., Carbajo, J., Hale, R.E., Harrison, T.J., Powers, J.J., Robb, K.R., Terrell, J.W., Wysocki, A.J., Greenwood, M.S.: Fluoride Salt-Cooled High-Temperature Demonstration Reactor Point Design. Oak Ridge National Laboratory (ORNL), Oak Ridge, TN (United States) (2016)
Rabiti, C.: RAVEN: Risk Analysis Virtual Environment. Idaho National Laboratory (2018)
Rabiti, C., Epiney, A.S., Talbot, P., Kim, J.S., Guler Yigitoglu, A., Greenwood, M.S., Cetiner, S.M., Ganda, F., Maronati, G.: Status Report on Modelling and Simulation Capabilities for Nuclear-Renewable Hybrid Energy Systems. Idaho National Laboratory (2017)
Rader, J., Greenwood, M.S.: Verification of Modelica-Based Models with Analytical Solutions for Tritium Diffusion. Nucl. Technol. (2018)
Robertson, R.C.: Conceptual Design Study of a Single-Fluid Molten-Salt Breeder Reactor. Oak Ridge National Laboratory (1971)
Rosenthal, M.W.: An Account of Oak Ridge National Laboratory's Thirteen Research Reactors. Oak Ridge National Laboratory (ORNL); High Flux Isotope Reactor (2009)
Sjölund, M., Gebremedhin, M., Fritzson, P.: Parallelizing Equation-Based Models for Simulation on Multi-Core Platforms by Utilizing Model Structure. In: Proceedings of the 17th International Workshop on Compilers for Parallel Computing. p. 5. , Lyon, France (2013)
Smith, J., Simmons, W.E.: An Assessment of a 2500 MWe Molten Chloride Salt Fast Reactor. Atomic Energy Establishment Winfrith, United Kingdom (1974)
Stempien, J.D.: Tritium Transport, Corrosion, and Fuel Performance Modeling in the Fluoride Salt-Cooled High-Temperature Reactor (FHR), (2015)
Sun, C.L., Chen, J.C., Yu, Y.W., Ha, H.C., Lu, C.S., Lee, T.Y.: Dynamic adsorption properties of Kr and Xe isotopes in charcoal. J. Radioanal. Nucl. Chem. 181, 291–299 (1994). doi:10.1007/BF02037635
Taube, M., Ligou, J., Ottewitte, E.H., Stepanek, J., Bucher, K.H., Dawudi, M., Janovici, E., Furrer, M.: Fast Reactors Using Molten Chloride Salts as Fuel. Swiss Federal Institute for Reactor Research (1978)

Touran, N.W., Gilleland, J., Malmgren, G.T., Whitmer, C., Gates, W.H.: Computational Tools for the Integrated Design of Advanced Nuclear Reactors. Engineering. 3, 518–526 (2017). doi:10.1016/J.ENG.2017.04.016

Yoder, G.L.: Examination of Liquid Fluoride Salt Heat Transfer. In: Proceedings of ICAPP 2014. , Charlotte, NC, USA (2014)

Functional Mock-up Interface, http://fmi-standard.org/